Monthly Notices
of the
ROYAL ASTRONOMICAL SOCIETY

Mon. Not. R. Astron. Soc. **421,** 2982–2997 (2012) doi:10.1111/j.1365-2966.2012.20524.x

What drives the ultraviolet colours of passive galaxies?

Russell J. Smith,[1⋆] John R. Lucey[1] and David Carter[2]

[1]*Department of Physics, Science Laboratories, University of Durham, Durham DH1 3LE*
[2]*Astrophysics Research Institute, Liverpool John Moores University, Twelve Quays House, Egerton Wharf, Birkenhead CH41 1LD*

Accepted 2012 January 9. Received 2012 January 6; in original form 2011 October 25

ABSTRACT

We present and analyse optical and ultraviolet (UV) colours for passive and optically-red Coma cluster galaxies for which we have spectroscopic age and element abundance estimates. Our sample of 150 objects covers a wide range in mass, from giant ellipticals down to the bright end of the dwarf-galaxy regime. Galaxies with ongoing star formation have been removed using strict Hα emission-line criteria. We focus on the colours $FUV - i$, $NUV - i$, $FUV - NUV$, $u^* - g$ and $g - i$. We find that all of these colours are correlated with both luminosity and velocity dispersion at the $>5\sigma$ level, with $FUV - i$ and $FUV - NUV$ becoming bluer with increasing 'mass' while the other colours become redder. We perform a purely empirical analysis to assess what fraction of the variation in each colour can be accounted for by variations in the average stellar populations, as traced by the optical spectra. For the optical colours, $u^* - g$ and $g - i$, most of the observed scatter ($\sim$80 per cent after allowing for measurement errors and for systematic errors in $u^* - g$) is attributable to stellar population variations, with colours becoming redder with increasing age and metallicity (Mg/H). The $FUV - i$ colour becomes bluer with increasing age and with increasing Mg/H, favouring the 'metal-rich single-star' origin for the UV upturn. However, correlations with the optically-dominant stellar populations account for only about half of the large observed scatter. We propose that the excess scatter in $FUV - i$ may be due to a varying proportion of ancient stars in galaxies with younger [simple stellar population (SSP) equivalent] average ages. The $NUV - i$ colour is sensitive to SSP-equivalent age and Mg/H (in the same sense as optical colours), but also exhibits excess scatter that can be attributed to 'leakage' of the far-UV-dominant (FUV-dominant) old hot population. After applying a correction based on the $FUV - i$ colour, the much of the remaining variance in $NUV - i$ is attributable to variations in the spectroscopic parameters, similar to the results for optical colours. Finally, the $FUV - NUV$ colour is surprisingly well behaved, showing strong correlations with age and metallicity, and little residual scatter. Interpreting this colour is complicated, however, since it mixes the effects of the main-sequence turn-off, in the near-UV, with the variation in the hot post-red giant branch content dominating the FUV.

Key words: galaxies: elliptical and lenticular, cD – galaxies: stellar content – ultraviolet: galaxies.

1 INTRODUCTION

The optical and near-infrared (near-IR) luminosities of old ($\gtrsim$3 Gyr) stellar populations are dominated by main-sequence, subgiant and red giant branch (RGB) stars, with a combined contribution of $\sim$80 per cent (Maraston 2005). In the ultraviolet (UV) regime, by contrast, these fairly well constrained evolutionary phases are faint, and the total light output becomes sensitive to hot post-RGB phases that are much less well understood.

In particular, the spectral energy distributions (SEDs) of many giant ellipticals and spiral bulges exhibit an 'upturn' in the far-UV (FUV) below $\sim$2000 Å (Code & Welch 1979). Early UV spectroscopy (e.g. Welch 1982; Ferguson et al. 1991) and imaging (e.g. Bohlin et al. 1985; O'Connell et al. 1992) showed that the upturn was not due to young massive stars, and hence low-mass evolved stars in old stellar populations are required (see O'Connell 1999 for an extensive review). The favoured candidate sources for the UV upturn are extreme horizontal branch (EHB) stars, and their hot post-HB descendants (Greggio & Renzini 1990), which have temperatures $T_{\rm eff} \approx 25\,000$ K. Such stars are observed in globular clusters, and also in the field, where they are designated subdwarf

⋆E-mail: russell.smith@durham.ac.uk

B stars (see Catelan 2009 for a review of the EHB among other HB phenomena). Their formation is thought to require either large mass loss on the RGB, occurring at high metallicity[1] (Greggio & Renzini 1990; Yi, Demarque & Kim 1997a) or through a variety of binary interactions (Han, Podsiadlowski & Lynas-Gray 2007). An unresolved question is the degree to which these rather exotic stellar phenomena are related, on a broad scale, to the properties of the stellar populations which dominate the optical light of the same galaxies.

Observationally, one way to explore the systematic variation in FUV output for (optically) red galaxies is to compare UV colours against luminosity and velocity dispersion, by analogy with the tight scaling relations obtained for optical colours. However, a more direct test for the physical origin of the UV flux is to compare against indicators for the age and metallicity of the stellar populations that dominate in the optical. Optical colours and individual absorption line strengths (e.g. Mgb or Hβ) provide some constraints on the stellar populations, but are always sensitive to a combination of both age and metallicity effects. An alternative method, pursued in this paper, is to correlate the UV colours against ages, metallicities and element abundance ratios derived from line indices, through comparison to spectral synthesis models. This is by no means the first attempt to address these questions, and we review some relevant previous work in the following paragraphs.

Using observations of 31 early-type galaxies with the *International Ultraviolet Explorer*, Burstein et al. (1988) showed that the $FUV - V$ colour becomes bluer with increasing velocity dispersion, σ, as the upturn component strengthens in the most massive galaxies. Moreover, the same colour was found to be anticorrelated with the Lick Mg_2 absorption index. Since this index is primarily a metallicity indicator (although also sensitive to age) Burstein et al. concluded that metallicity is the fundamental parameter underlying the observed correlations. O'Connell (1999) repeated this test with a larger set of line indices from Trager et al. (1998), and found that $FUV - V$ shows clear trends with indices tracing light-element abundances, but is essentially uncorrelated with indices dominated by iron abundance.

A dramatic improvement in the systematic study of UV emission from passive galaxies was enabled by the *Galaxy Evolution Explorer* (*GALEX*) satellite (Martin et al. 2005; Morrissey et al. 2007), with its wide field of view and two-channel imaging capability [near-UV (NUV): $\lambda_{\rm eff} = 2310$ Å; far-UV (FUV): $\lambda_{\rm eff} = 1530$ Å]. In an early study of UV colours of 'quiescent early-type' galaxies with *GALEX*, Rich et al. (2005) concluded that there was 'no correlation between the $FUV - r$ colour and any parameter sensitive to the global metallicity', including the Mg_2 index used by Burstein et al. (1988). The Rich et al. sample was limited to luminous galaxies, with essentially no coverage at $\sigma < 100\,{\rm km\,s^{-1}}$. Other early *GALEX* studies by Boselli et al. (2005) and Donas et al. (2007) focused on nearby galaxies, and covered a wider range in luminosity. Both works recovered correlations between $FUV - NUV$ and Mg_2, in the sense observed by Burstein et al. (1988), although Donas et al. show that the correlation is much weaker for $FUV - V$. They emphasize that the tight correlation in $FUV - NUV$ is likely driven by metal-line blanketing in the NUV from the main-sequence turn-off stars, rather than by variation in the hot UV-upturn sources.

More recently, Bureau et al. (2011, hereafter B11) have revisited this issue using *GALEX* colours combined with SAURON integral-field spectroscopy, for a sample of 48 very nearby early-type galaxies. Their analysis has an advantage over previous work, in that colours and spectroscopic parameters can be extracted at identical apertures. After excluding galaxies with strong Hβ absorption, indicative of recent star formation, B11 find that galaxies with bluer $FUV - V$ have stronger Mgb, similar to the original result of Burstein et al. (Note that B11 follow Burstein et al. in treating colour as an independent variable in the regression.) They also find that galaxies with bluer $FUV - V$ have lower Hβ absorption, suggesting older populations or higher metallicity, while there is no clear trend for Fe5015, an iron-dominated index. They conclude that α-element abundance or total metallicity is an important driver of the UV upturn.

Although Mgb (like Mg_2) is considered primarily a metallicity indicator, it also depends on age. Hence, a correlation of the $FUV -$ optical colour with this index does not unambiguously signal that the UV upturn depends on metallicity. Comparison of the UV colours against stellar population parameters (age, metallicity, etc.) estimated from multiple indices should help separate the effects of the physically meaningful quantities. This was attempted for the $NUV - J$ colour by Rawle et al. (2008), who concluded that metallicity effects were dominant in driving the systematic variation in this colour, with a residual dependence on age, while a large (0.25 mag) excess scatter remained unexplained by the correlations. Loubser & Sánchez-Blázquez (2011) performed similar comparisons for a sample of brightest cluster galaxies (BCGs) and a control sample of similarly massive ellipticals that are not BCGs. They found no significant correlations of $FUV - NUV$ either with line strength indices (including Mgb5177), or with age, metallicity (Z/H) or abundance ratio α/Fe taken individually. The construction of their sample, by its nature, limits the baseline in mass and stellar population properties which would be necessary to constrain any such correlations. Carter et al. (2011) have applied a similar method for a sample of nearby ellipticals with spectroscopic parameters compiled from a range of literature sources. Testing for correlation with each single parameter in turn, they found significant negative correlations of $FUV - NUV$ with total metallicity (Z/H), and with α/Fe but not with iron abundance (Fe/H); the age dependence was not explored.

In this paper, we use deep *GALEX* imaging of the Coma cluster, together with optical data from the Canada–France–Hawaii Telescope (CFHT) and the Sloan Digital Sky Survey (SDSS), to measure UV and optical colours for a sample of red-sequence galaxies for which ages, metallicities and abundance ratios have been determined from high-S/N spectroscopy. The key improvements over previous works are (1) the use of (in principle) meaningful stellar population parameters, rather than individual indices which mix age and metallicity effects, and (2) application to a sample spanning a wide range in galaxy mass ($\sigma = 50$–$400\,{\rm km\,s^{-1}}$). We analyse the correlations of the colours with spectroscopic ages and abundances, making use of multiparametric fits to disentangle the effects of each parameter. In particular, we aim to determine what fraction of the variation in each colour is driven by variations in the stellar populations, as constrained from the optical, and what fraction is 'excess scatter', apparently unrelated to the optically-dominant populations. Our approach is purely empirical, and independent of any population synthesis models for the UV colours.

[1] The formation of EHB stars in low-metallicity populations appeared unable to reproduce the upturn without adopting unrealistically high ages. Chung et al. (2011) have recently argued that helium-enhanced subpopulations (for which there is independent evidence in some globular clusters) can develop a strong upturn at ages less than the Hubble time, since main-sequence lifetimes are shorter for higher helium abundances.

The structure of this paper is as follows. The optical spectroscopy and the *GALEX* and optical imaging data are described in Section 2. The results from fitting the colours with single- and multi-parameter models are presented in Section 3, together with an exploration of residual trends and tests for effects of systematic errors. We discuss the implications of our results in Section 4, focusing especially on the questions of the origin of the UV upturn, and whether the scatter in the NUV implies widespread recent star formation among optically passive galaxies. Our conclusions are summarized in Section 5.

2 DATA

Our approach is to measure UV/optical colours for galaxies drawn from a catalogue of galaxies with measured spectroscopic ages and metallicities. Full details of the spectroscopy are given in related papers (Smith et al. 2012; Smith et al., in preparation). Broadly the parent sample comprises spectra for 242 bright Coma cluster members from SDSS (analysed in Price et al. 2010) and 169 fainter members observed using long integrations with Hectospec at the 6.5-m MMT. The MMT sample is an extended version of that reported by Smith et al. (2009). Velocity dispersions were compiled from a variety of literature sources, supplemented with new observations from VLT/FLAMES, and combined using observations from multiple data sources to determine relative systematic offsets.

The combined MMT and SDSS sample has been homogeneously re-analysed, to measure absorption-line strength indices and emission-line equivalent widths (used in defining a passive galaxy sample). Ages, metallicities (Fe/H) and abundance ratios (Mg/Fe, Ca/Fe, C/Fe and N/Fe) were measured via comparison to the Schiavon (2007) simple stellar population (SSP) models, using a new model inversion code. The first step in this process is a non-linear optimization to derive Fe/H and age assuming solar abundance ratios, using the observed Hβ and $\langle\mathrm{Fe}\rangle = \frac{1}{2}$(Fe5270+Fe5335) indices. Then we use a fast linear fit (i.e. a matrix inversion) to estimate a correction to the abundance pattern required to match additional indices (Mgb, Ca4227, $C_2$4668 and CN_2), at the fitted age and Fe/H. Using this updated abundance pattern, we repeat the non-linear fit to obtain an improved estimate of the age and Fe/H. Alternating between these steps, the process converges within a few iterations. Parameter errors (and covariances) are obtained by propagating the index errors through the fitting process using Monte Carlo simulations (50 realizations per galaxy). We allow extrapolation of predictions beyond the model limits (e.g. to unphysically large ages), in order to characterize the errors correctly. We have confirmed that our method yields results consistent with the much slower method of Graves & Schiavon (2008), when applied to the same data. The derived properties (especially age) should be interpreted as 'SSP-equivalent parameters', that is, they are the parameters of the single-burst, single-metallicity, single-abundance-mixture population which best reproduces the measured indices.

We draw the UV data from proprietary and archival *GALEX* observations in the NUV and FUV. There are two deep observations: GI5_025001_COMA with 15-ks integration in the cluster core (see also Smith et al. 2010) and GI2_046001_COMA3 with 30-ks exposure in a field centred 0.°9 to the south-west (see also Hammer et al. 2010). Retrieving additional archival tiles with integration times 1–5 ks from the archive resulted in coverage for almost all galaxies in our spectroscopic sample. For galaxies covered by more than one *GALEX* tile, we employ only the deepest available observation. Deep observations with *GALEX* are confusion limited, and many of the faintest objects in our sample would not be individually detected by running, for example, SExtractor (Bertin & Arnouts 1996) on the *GALEX* images. Instead, we simply extract the UV fluxes from circular apertures with centres fixed at the optical coordinates. We adopt an aperture of 10 arcsec diameter, corresponding to ∼5 kpc at the distance of Coma, which is sufficiently large to avoid sensitivity to variation in the *GALEX* point spread function (PSF; 5–6 arcsec full width at half-maximum). A local sky estimate is obtained from an annulus of radius 30–60 arcsec, with contaminating sources identified by $k\sigma$ clipping the (deeper) NUV images, and subsequently excised from the sky statistics in both bands.

For optical photometry in redder passbands, we use aperture magnitudes from the 7th Data Release of the SDSS, for the g and i bands, interpolating from the published apertures to the 10 arcsec diameter used for the UV. Since the SDSS u-band photometry is very shallow, we instead use dedicated observations obtained with MegaCam at CFHT. The CFHT u^*-band imaging covers a 2.8 × 2.8 deg^2 area with a grid of nine slightly overlapping pointings. The u^* filter is ∼200 Å redder than SDSS u. The individual exposures for each ∼1 deg^2 pointing were processed and stacked at the observatory using the Elixir pipeline (Magnier & Cuillandre 2004). Magnitudes in 10-arcsec apertures were measured from the stacks, which have a total exposure time of 1360 s.

The adopted random errors in the aperture magnitudes and colours include contributions from photon statistics and from confusion noise. We estimate the latter in all five bands, by measuring the 68 percentile interval of the total flux in 10-arcsec apertures placed randomly in a representative image, and propagating the effects into errors as a function of galaxy magnitude. Confusion noise is the dominant source of random error in the UV for the deepest *GALEX* tiles, due to the low spatial resolution of the images, and also because the cluster galaxies are relatively faint in the UV compared to the background sources. Even in the optical, however, confusion can be comparable to the (generally very small) photon errors, given the large apertures used for the photometry. The adopted errors do not include contributions from systematic calibration error, since many of the galaxies in the sample are drawn from only a small number of observations (i.e. *GALEX* tiles, SDSS drift-scan runs, MegaCam pointings) per data source, and hence calibration errors affect large parts of the sample coherently. We assess the impact of systematic calibration errors in Section 3.4.1 by explicitly allowing additional 'offset' terms in our analysis.

No corrections for Galactic extinction are applied. At the high Galactic latitude of Coma, the mean reddening from Schlegel, Finkbeiner & Davis (1998) is $\langle E(B-V)\rangle = 0.01$ mag, with a galaxy-to-galaxy scatter of 0.001 mag. Even in the NUV (the band most sensitive to extinction), this would introduce a scatter of <0.01 mag in flux, which is negligible in comparison to the observed scatter (∼0.2 mag). No k-corrections are applied, since they are necessarily model-dependent and very uncertain in the UV bands. Although all sample galaxies lie at approximately the same distance, their recession velocities span a range 3800–9400 km s^{-1}. Hence, band shifting effects may be relevant, for example, in the u^* band, where the long-wavelength filter cut-off is close to the steep 4000 Å break. We address this point in Section 3.4.2 by testing fits which explicitly include a redshift-dependent term.

From the full spectroscopic data set, we restrict the sample to galaxies having age greater than 2 Gyr, error less than 0.3 in $\log t_{\rm ssp}$ and [Mg/H], and FUV error less than 0.3 mag. Furthermore, we retain only galaxies with measured velocity dispersions,

and with <0.5 Å equivalent width in Hα emission (after separation from the absorption line). The purpose of the Hα cut is primarily to remove galaxies in which the stellar Hβ absorption line, used in the estimation of ages and metallicities, is contaminated by nebular emission. In addition, the selection against Hα emission helps to remove objects whose UV colours are influenced by ongoing star formation in their central regions. (We address the possibility of star formation beyond the spectroscopic fibre in Section 3.4.3.) We automatically reject galaxies with UV flux centroids offset from the nominal galaxy position by more than 1.5 arcsec, to select against objects contaminated by neighbouring sources. (The centroid shift threshold is supported by simulations of isolated Poisson-sampled PSFs, tuned to the depth of the shallower tiles.) Finally, all remaining sources were inspected visually on the *GALEX* and optical images, and five galaxies manually removed from the sample due to blending undetected by the centroid offset, or location within the halo of a UV-bright star.

The resulting sample comprises 150 galaxies. For 90 objects (60 per cent), the UV measurements are from the deep Coma Core tile, while for 25 (17 per cent), the UV data are from the deep Coma South West tile. The remaining 35 objects (23 per cent) are from the shallower tiles. The merged sample is mainly (97 per cent) comprised of galaxies with SDSS spectroscopy, since the UV flux errors are typically too large for the fainter galaxies observed that were observed with MMT. The final data set used for the analysis in this paper is reported in Tables 1 and 2. Note that the derived parameters for SDSS galaxies differ slightly from those tabulated in Price et al. (2010) due to different conventions and methods adopted in re-analysing the index data.

3 LINEAR ANALYSIS OF THE COLOURS

3.1 Methodology

In this paper, we take a purely empirical and statistical approach to assessing the extent to which variations in various physical parameters can account for the variation in the UV and optical colours of non-star-forming galaxies. We make no use of population synthesis models to predict the colours. Instead, we perform linear regression analyses, seeking to find the predictor variable (or variables) which best reproduce the observed colours.

We restrict attention to a subset of colours chosen to highlight the behaviour in the UV in comparison to the optical, with little redundancy:

(i) $FUV - i$: directly probes the UV-upturn sources, measuring the flux from old hot stars versus that from old cool stars.
(ii) $NUV - i$: the NUV flux likely has contributions from the main-sequence turn-off as well as from the upturn sources.
(iii) $FUV - NUV$: a colour measurable from *GALEX* alone.
(iv) $u^* - g$: a blue-optical colour, measuring the 4000 Å break, to test the transition between UV and optical regimes.
(v) $g - i$: a broad optical colour for comparison.

We fit the observed colours to the following linear models in which the predicted colour is p, given by

$$p = a_{0,L} + a_L \log(L_r/10^{10} L_{r,\odot}),$$

$$p = a_{0,\sigma} + a_\sigma \log(\sigma/100\,\mathrm{km\,s^{-1}}),$$

Table 1. The galaxy properties used for the analysis in Section 3. The identifications are from Godwin, Metcalfe & Peach (1983), where available, with coordinates derived from matching to SDSS. The parameters used as predictors for the colours are the r-band luminosity from SDSS (L_r), the velocity dispersion (σ) from the compilation in Smith et al. (2012), and the SSP-equivalent age and metallicity ($T_{\rm ssp}$ and [Mg/H]) from Smith et al. (2012). The errors on the latter parameters are highly anticorrelated. The error coefficient $\rho_{\rm err}$ is needed when computing errors on combinations of age and metallicity. The complete table is provided in the online version of the journal (see Supporting Information).

Galaxy	RA	Dec	$\log(L_r/L_\odot)$	$\log(\sigma/\mathrm{km\,s^{-1}})$	$\log(T_{\rm ssp}/10\,\mathrm{Gyr})$	[Mg/H]	$\rho_{\rm err}$
GMP 6617	12:54:05.52	+27:04:07.0	10.16	2.065 ± 0.015	0.920 ± 0.151	0.010 ± 0.109	−0.86
GMP 6568	12:54:09.98	+28:05:33.0	10.13	2.223 ± 0.011	0.948 ± 0.115	0.239 ± 0.077	−0.79
GMP 6545	12:54:16.03	+27:18:13.5	10.26	2.213 ± 0.014	0.737 ± 0.162	0.261 ± 0.116	−0.92
GMP 6503	12:54:22.28	+27:05:03.0	9.77	2.158 ± 0.013	1.012 ± 0.146	0.236 ± 0.107	−0.88
GMP 6404	12:54:32.96	+28:22:36.4	10.24	2.131 ± 0.014	0.877 ± 0.158	0.242 ± 0.095	−0.88
GMP 6409	12:54:36.82	+26:56:05.5	10.06	1.868 ± 0.029	0.581 ± 0.181	0.096 ± 0.150	−0.88
GMP 5978	12:55:27.79	+27:39:22.0	10.25	2.191 ± 0.013	0.893 ± 0.128	0.219 ± 0.090	−0.81
GMP 5975	12:55:29.10	+27:31:17.2	10.51	2.275 ± 0.004	0.810 ± 0.142	0.321 ± 0.079	−0.88
GMP 5886	12:55:41.30	+27:15:02.7	10.36	2.408 ± 0.010	1.099 ± 0.110	0.372 ± 0.083	−0.84
GMP 5704	12:56:01.75	+26:45:23.8	9.78	2.195 ± 0.015	1.044 ± 0.263	0.187 ± 0.140	−0.91
GMP 5641	12:56:06.40	+27:38:52.0	9.69	1.828 ± 0.034	0.330 ± 0.043	0.184 ± 0.039	−0.74
GMP 5599	12:56:09.90	+27:50:39.3	10.04	2.088 ± 0.013	0.801 ± 0.132	0.313 ± 0.081	−0.87
GMP 5526	12:56:16.69	+27:26:45.5	9.82	2.119 ± 0.013	0.991 ± 0.277	0.199 ± 0.179	−0.94
GMP 5495	12:56:19.79	+27:45:03.7	10.09	2.267 ± 0.013	1.046 ± 0.172	0.381 ± 0.113	−0.88
GMP 5428	12:56:26.63	+27:49:50.3	10.11	2.178 ± 0.010	1.011 ± 0.129	0.324 ± 0.096	−0.83
GMP 5424	12:56:29.13	+26:57:25.2	10.29	2.204 ± 0.012	0.884 ± 0.156	0.158 ± 0.094	−0.90
GMP 5397	12:56:29.82	+27:56:24.0	10.08	2.253 ± 0.010	1.089 ± 0.133	0.302 ± 0.100	−0.87
GMP 5395	12:56:32.04	+27:03:20.1	9.91	2.212 ± 0.010	0.935 ± 0.168	0.264 ± 0.094	−0.88
GMP 5364	12:56:34.19	+27:32:20.2	10.02	2.197 ± 0.009	0.848 ± 0.142	0.361 ± 0.103	−0.83
GMP 5341	12:56:35.20	+28:16:31.6	9.89	2.109 ± 0.016	0.766 ± 0.166	0.267 ± 0.110	−0.84
GMP 5272	12:56:42.86	+28:01:13.6	10.29	2.260 ± 0.010	1.023 ± 0.131	0.339 ± 0.093	−0.86
GMP 5283	12:56:43.52	+27:02:05.1	9.64	1.891 ± 0.029	0.799 ± 0.241	0.030 ± 0.142	−0.85
GMP 5279	12:56:43.52	+27:10:43.7	10.65	2.374 ± 0.003	1.102 ± 0.132	0.311 ± 0.085	−0.87
GMP 5250	12:56:47.77	+27:25:15.6	9.56	1.797 ± 0.027	0.510 ± 0.170	0.126 ± 0.137	−0.72
GMP 5191	12:56:53.14	+27:55:46.2	9.79	2.319 ± 0.013	1.247 ± 0.190	0.281 ± 0.138	−0.82

Table 2. The 10- arcsec-diameter aperture magnitudes from which colours were derived for the analysis in Section 3. The FUV and NUV magnitudes are from *GALEX*, *g* and *i* are from SDSS (interpolated from DR7 aperture photometry), and u^* is from CFHT (this passband is centred ∼200 Å redder than SDSS *u*). All magnitudes are on the AB system. The quoted errors include a contribution from confusion noise, but not for calibration uncertainty. Neither extinction corrections nor *k*-corrections have been applied. The complete table is provided in the online version of the journal (see Supporting Information).

Galaxy	*GALEX* tile	$FUV_{10\,\mathrm{arcsec}}$	$NUV_{10\,\mathrm{arcsec}}$	$u^*_{10\,\mathrm{arcsec}}$	$g_{10\,\mathrm{arcsec}}$	$i_{10\,\mathrm{arcsec}}$
GMP 6617	NGA_DDO154	22.525 ± 0.119	21.094 ± 0.043	17.257 ± 0.003	15.891 ± 0.002	14.724 ± 0.004
GMP 6568	GI1_039003_Coma_MOS03	22.141 ± 0.137	21.180 ± 0.052	17.225 ± 0.003	15.747 ± 0.002	14.545 ± 0.002
GMP 6545	NGA_DDO154	21.736 ± 0.074	20.701 ± 0.032	16.991 ± 0.002	15.590 ± 0.002	14.390 ± 0.001
GMP 6503	NGA_DDO154	22.903 ± 0.153	21.695 ± 0.068	17.754 ± 0.005	16.323 ± 0.003	15.116 ± 0.002
GMP 6404	GI1_039003_Coma_MOS03	22.308 ± 0.152	21.388 ± 0.061	17.444 ± 0.004	15.956 ± 0.002	14.744 ± 0.002
GMP 6409	NGA_DDO154	23.203 ± 0.187	21.403 ± 0.054	17.629 ± 0.004	16.389 ± 0.003	15.315 ± 0.003
GMP 5978	COMA_SPEC_A	22.325 ± 0.171	21.090 ± 0.048	17.129 ± 0.003	15.640 ± 0.002	14.435 ± 0.001
GMP 5975	GI2_046001_COMA3	21.710 ± 0.038	20.508 ± 0.020	16.382 ± 0.001	14.949 ± 0.011	13.742 ± 0.009
GMP 5886	GI2_046001_COMA3	20.551 ± 0.017	20.169 ± 0.015	16.623 ± 0.002	15.184 ± 0.001	13.943 ± 0.001
GMP 5704	GI2_046001_COMA3	22.544 ± 0.072	21.464 ± 0.046	17.595 ± 0.004	16.278 ± 0.003	15.095 ± 0.002
GMP 5641	GI2_046001_COMA3	23.742 ± 0.194	21.759 ± 0.059	17.922 ± 0.005	16.613 ± 0.004	15.591 ± 0.004
GMP 5599	COMA_SPEC_A	22.996 ± 0.261	21.513 ± 0.065	17.744 ± 0.005	16.233 ± 0.003	15.014 ± 0.002
GMP 5526	GI2_046001_COMA3	23.188 ± 0.121	21.740 ± 0.058	17.824 ± 0.005	16.474 ± 0.003	15.291 ± 0.003
GMP 5495	COMA_SPEC_A	22.064 ± 0.150	21.034 ± 0.046	17.198 ± 0.003	15.659 ± 0.002	14.432 ± 0.001
GMP 5428	COMA_SPEC_A	22.301 ± 0.169	21.048 ± 0.047	17.273 ± 0.003	15.788 ± 0.002	14.590 ± 0.002
GMP 5424	GI2_046001_COMA3	22.046 ± 0.049	20.637 ± 0.022	16.757 ± 0.002	15.405 ± 0.002	14.221 ± 0.001
GMP 5397	GI1_039003_Coma_MOS03	21.967 ± 0.125	21.165 ± 0.052	17.442 ± 0.003	15.960 ± 0.003	14.762 ± 0.003
GMP 5395	GI2_046001_COMA3	22.681 ± 0.080	21.068 ± 0.032	17.207 ± 0.003	15.881 ± 0.002	14.741 ± 0.002
GMP 5364	GI2_046001_COMA3	22.278 ± 0.058	21.335 ± 0.041	17.411 ± 0.003	15.980 ± 0.002	14.745 ± 0.002
GMP 5341	GI1_039003_Coma_MOS03	23.093 ± 0.241	21.582 ± 0.070	17.626 ± 0.004	16.208 ± 0.003	15.031 ± 0.002
GMP 5272	GI1_039003_Coma_MOS03	21.918 ± 0.122	20.959 ± 0.045	17.072 ± 0.002	15.575 ± 0.002	14.343 ± 0.001
GMP 5283	GI2_046001_COMA3	23.728 ± 0.191	21.535 ± 0.049	17.837 ± 0.005	16.603 ± 0.004	15.519 ± 0.003
GMP 5279	GI2_046001_COMA3	20.808 ± 0.020	20.120 ± 0.015	16.428 ± 0.001	14.952 ± 0.001	13.693 ± 0.001
GMP 5250	GI2_046001_COMA3	23.960 ± 0.233	21.833 ± 0.063	18.136 ± 0.007	16.954 ± 0.005	15.928 ± 0.005
GMP 5191	COMA_SPEC_A	22.263 ± 0.167	21.278 ± 0.055	17.552 ± 0.004	16.105 ± 0.003	14.899 ± 0.002

$$p = a_{0,t} + a_t \log(T_{\rm ssp}/10\,{\rm Gyr}),$$

$$p = a_{0,Z} + a_Z[{\rm Mg/H}],$$

$$p = a_{0,tZ} + a_t \log(T_{\rm ssp}/10\,{\rm Gyr}) + a_Z[{\rm Mg/H}],$$

where σ is velocity dispersion, L_r is total *r*-band luminosity, $T_{\rm ssp}$ is spectroscopic age and [Mg/H] is spectroscopic Mg abundance, which is close to the total metallicity, *Z*/H. The coefficients *a* are determined by *minimizing the scatter in colour*; this approach differs from some previous analyses (e.g. B11).

We quantify the fits primarily through the 'coefficient of determination', R^2, defined as the fraction of total variance in the colour which is accounted for by correlations with the predictor variable:

$$R^2 = 1 - \frac{\sum_i (y_i - p_i)^2}{\sum_i (y_i - \bar{y})^2} = 1 - \frac{\sigma^2_{\rm residual}}{\sigma^2_{\rm total}}.$$

Here, y_i are the measured colours and p_i are the colours predicted from a linear model, for example, in the case of a fit to SSP-equivalent age. As indicated in the second expression, $1 - R^2$ is the ratio of the residual variance around the fit to the total variance in the colour.

We also use a generalization of the above to account for measurement errors:

$$T^2 = R^2 + \frac{\sum_i e^2_{y,i} + e^2_{p,i}}{\sum_i (y_i - \bar{y})^2} = 1 - \left(\frac{\sigma^2_{\rm residual}}{\sigma^2_{\rm total}} - \frac{\sigma^2_{\rm errors}}{\sigma^2_{\rm total}} \right)$$

where $e_{y,i}$ are the errors in measured colour and $e_{p,i}$ are the errors in the predicted colour, for example, $e_p = a_t e_{\log t_{\rm ssp}}$ in the case of the fit to age. T^2 thus represents the fraction of the total variance (in observed colour) which is attributable to a combination of (i) the correlations with the predictor variables, and (ii) the measurement errors, both in colour and in the predictors.

3.2 Observed colours versus luminosity and velocity dispersion

We begin by briefly considering the colour–luminosity and colour–σ relations, as shown in Fig. 1. The slopes and other parameters of the fits are reported in Table 3.

The colour–luminosity relations (upper panels of Fig. 1) show the familiar results that $FUV - i$ and $FUV - NUV$ become *bluer* with increasing luminosity, contrary to the behaviour of colours at longer wavelengths. Galaxies with $FUV - NUV < 0.9$ have a 'classical' UV upturn, in the sense of having rising spectra (f_λ versus λ) in the UV regime. Such colours are seen mainly at the bright end of the luminosity distribution. Our approach is to treat the galaxy population continuously, rather than assign any particular significance to this value. For reference, however, we distinguish the 14 objects with $FUV - NUV < 0.9$ using different symbols in this and subsequent figures.[2]

The colour–luminosity relations show that the UV colours exhibit much greater scatter (0.2–0.3 mag) than the optical colours (∼0.05 mag). In part, this difference in the absolute value of the scatter is trivially accounted for by the much larger total colour range spanned by the sample. The quantities R^2 and T^2 scale this out by comparing the variance around the fit to the total variance in colour. The R^2 values indicate that the luminosity dependence

[2] We note that Yi et al. (2011) found no bright Coma ellipticals satisfying $FUV - NUV < 0.9$. The apparent discrepancy is probably due to the *k*-corrections applied in that work but not here.

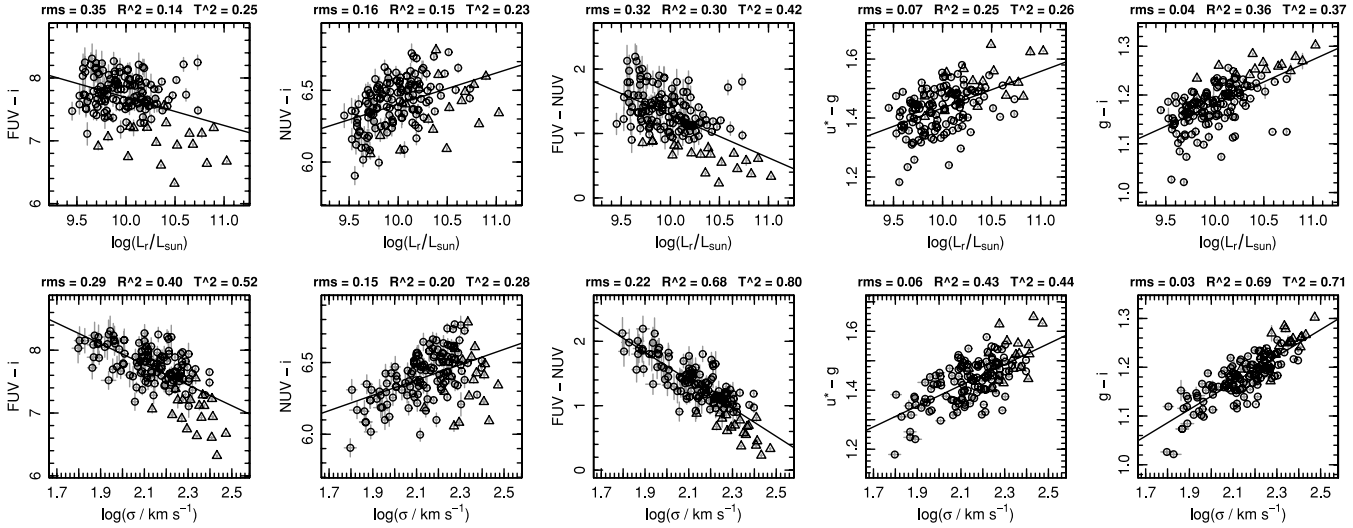

Figure 1. UV and optical colours as a function of optical luminosity L_r (upper panels) and velocity dispersion σ (lower panels). The solid line in each panel is the linear fit as recorded in Table 3. The header line indicates the rms scatter about the fit, the coefficient of determination R^2 (the fraction of total variance in the colour that is accounted for by the correlation), and the T^2 parameter which is equivalent to R^2 but includes the effect of measurement errors. The galaxies marked with the triangular symbols have $FUV - NUV < 0.9$, indicating that they are classical UV-upturn galaxies.

Table 3. Parameters of linear fits to the observed colours. For each colour, the six lines give the results for (1) a null model fitting only a mean value; (2) a fit against luminosity; (3) a fit against velocity dispersion; (4) a fit against spectroscopic age; (5) a fit against spectroscopic metallicity; and (6) a simultaneous fit to age and metallicity. The coefficients a refer to a general model of the form $p = a_0 + a_L \log(L_r/(10^{10}\,\mathrm{L}_\odot)) + a_\sigma \log(\sigma/100\,\mathrm{km\,s^{-1}}) + a_t \log(t_{\rm ssp}/10\,\mathrm{Gyr}) + a_Z[\mathrm{Mg/H}]$, although only subsets of these terms are used in each fit. For each line, the quantity R^2 is the ratio of the total variance explained by the fitted model. T^2 is the fraction of variance explained by the fitted model *and* the nominal measurement errors in both the colours and the predictor variables.

Colour	a_0	a_L	a_σ	a_t	a_Z	rms	R^2	T^2
$FUV - i$	7.683 ± 0.002	–	–	–	–	0.373	–	–
	7.691 ± 0.028	-0.447 ± 0.090	–	–	–	0.346	0.14	0.25
	7.937 ± 0.035	–	-1.643 ± 0.163	–	–	0.287	0.41	0.52
	7.605 ± 0.028	–	–	-0.987 ± 0.126	–	0.314	0.29	0.61
	7.850 ± 0.071	–	–	–	-0.752 ± 0.290	0.365	0.04	0.21
	7.851 ± 0.057	–	–	-1.092 ± 0.119	-1.144 ± 0.236	0.291	0.39	0.58
$NUV - i$	6.407 ± 0.024	–	–	–	–	0.171	–	–
	6.404 ± 0.013	$+0.217 \pm 0.041$	–	–	–	0.157	0.16	0.24
	6.325 ± 0.018	–	$+0.534 \pm 0.087$	–	–	0.153	0.20	0.28
	6.420 ± 0.015	–	–	$+0.158 \pm 0.067$	–	0.168	0.04	0.14
	6.272 ± 0.031	–	–	–	$+0.612 \pm 0.126$	0.159	0.14	0.38
	6.271 ± 0.030	–	–	$+0.221 \pm 0.062$	$+0.691 \pm 0.124$	0.153	0.20	0.37
$FUV - NUV$	1.275 ± 0.012	–	–	–	–	0.382	–	–
	1.287 ± 0.026	-0.664 ± 0.083	–	–	–	0.320	0.30	0.42
	1.613 ± 0.026	–	-2.177 ± 0.123	–	–	0.216	0.68	0.81
	1.185 ± 0.026	–	–	-1.145 ± 0.121	–	0.302	0.38	0.76
	1.578 ± 0.069	–	–	–	-1.364 ± 0.282	0.355	0.14	0.42
	1.580 ± 0.046	–	–	-1.312 ± 0.097	-1.835 ± 0.192	0.237	0.62	0.83
$u^* - g$	1.436 ± 0.019	–	–	–	–	0.077	–	–
	1.434 ± 0.005	$+0.124 \pm 0.017$	–	–	–	0.067	0.26	0.26
	1.382 ± 0.007	–	$+0.353 \pm 0.033$	–	–	0.058	0.44	0.45
	1.449 ± 0.006	–	–	$+0.168 \pm 0.028$	–	0.069	0.20	0.34
	1.370 ± 0.014	–	–	–	$+0.300 \pm 0.056$	0.071	0.16	0.36
	1.369 ± 0.011	–	–	$+0.202 \pm 0.024$	$+0.373 \pm 0.047$	0.058	0.44	0.53
$g - i$	1.183 ± 0.005	–	–	–	–	0.048	–	–
	1.181 ± 0.003	$+0.091 \pm 0.010$	–	–	–	0.038	0.36	0.38
	1.141 ± 0.003	–	$+0.273 \pm 0.015$	–	–	0.026	0.69	0.71
	1.194 ± 0.003	–	–	$+0.137 \pm 0.015$	–	0.038	0.35	0.61
	1.140 ± 0.008	–	–	–	$+0.191 \pm 0.034$	0.043	0.17	0.40
	1.140 ± 0.006	–	–	$+0.160 \pm 0.012$	$+0.249 \pm 0.023$	0.029	0.63	0.74

accounts for only ∼15 per cent of the total variance in the 'UV-to-optical' colours $FUV - i$ and $NUV - i$. Luminosity correlations account for a larger fraction of variance in the 'optical-to-optical' colours $u^* - g$ (25 per cent) and $g - i$ (36 per cent). Perhaps surprisingly, the luminosity trend also accounts for 30 per cent of the scatter in the 'UV-to-UV' colour, $FUV - NUV$. We will find throughout this paper that $FUV - NUV$ follows tighter correlations than the UV-to-optical colours. The T^2 values show that measurement errors contribute an additional ∼10 per cent of the total variance in the UV colours, but make negligible impact on the optical scatter.

As noted in previous work (e.g. Carter et al. 2011; Marino et al. 2011), the trends of UV colours with velocity dispersion are tighter than those with luminosity. The scalings with velocity dispersion, combined with the measurement errors, account for around 70 per cent of the variance in $g - i$ and $FUV - NUV$, but only 30–50 per cent of the variance in $FUV - i$, $NUV - i$ and $u^* - g$. Fitting simultaneously to σ and L_r (not given in the table or figures) indicates there is no significant dependence on luminosity at fixed velocity dispersion, consistent with results in the optical (Bernardi et al. 2005; Graves, Faber & Schiavon 2009).

To summarize, all colours are strongly correlated (at the $\gtrsim 5\sigma$ level) with optical luminosity and velocity dispersion. These correlations account for a much of the observed variance in the $g - i$ and $FUV - NUV$ colours, but significant excess scatter remains in $u^* - g$ and in the UV-to-optical colours.

3.3 Observed colours versus age and metallicity

We assume that the trends of colour with luminosity and velocity dispersion result from underlying variation in the *average* stellar populations in galaxies as a function of these quantities. In this section, we use the spectroscopic ages and metallicities to explore the degree to which such correlations can explain the observed colour variation.

In the absence of photometric errors (and of internal reddening or non-stellar flux sources such as active nuclei), the colours should be completely determined from the stellar populations present. In practice, however, we do not have full information about these populations. The spectroscopic data provide only a single characteristic age and metallicity, and estimates for abundance ratios of a few elements. At best, these are only moments of the true distribution in these parameters (e.g. $T_{\rm ssp}$ is weighted to the age of the most recent star formation episodes). An important caveat, in the context of this paper, is that if the UV colours are driven by subpopulations far from the average population, such as the very oldest or youngest stars, or the low- or high-metallicity 'tail' of the metallicity distribution, then this may not be reflected cleanly in correlations with average SSP-equivalent properties. However, spectroscopic age and metallicity are still more likely to reflect meaningful information about the galaxies than using individual line index strengths, which always depend on combinations of these parameters, as well as on individual element abundances. At worst, the SSP-equivalent parameters may be influenced by effects that are not adequately taken into account in the analysis used to derive them. For example, the measured 'age' may partly depend on the incidence of blue HB stars (e.g. Lee, Yoon & Lee 2000; Schiavon et al. 2004; Percival & Salaris 2011), as well as the main-sequence turn-off mass. Even in this case, however, the optical age and metallicity provide a useful compression of the spectroscopic constraints on the stellar content that are available from the optical light.

To test for correlations between the colours and the stellar populations which dominate the spectra, we fit colour versus age and metallicity (Mg/H), first individually, and then in linear combination. We use Mg/H as the primary metallicity tracer, rather than Fe/H, since the abundance of α elements better reflects the total metallicity Z/H (due to the large contribution of oxygen to the total number fraction in metals). The results are shown in Fig. 2, and the fit results summarized in Table 3.

The top row of panels in Fig. 2 show that $u^* - g$, $g - i$ and $NUV - i$ all become redder with increasing age, while $FUV - NUV$ and $FUV - i$ become bluer with increasing age. The coefficient of age is significant at the $>6\sigma$ level for all colours except $NUV - i$, where the correlation is only marginally significant (2.4σ). In $FUV - i$, we note an apparent steepening of the age dependence among the oldest galaxies. For $T_{\rm ssp} > 9$ Gyr (the median age of the sample galaxies), the slope is -1.50 ± 0.35 mag per decade in age, while for $T_{\rm ssp} < 9$ Gyr the slope is shallower and barely significant, at -0.39 ± 0.21 mag per decade. According to R^2 (i.e. without accounting for measurement errors), the linear age trends make 20–40 per cent contributions to the total variance in the colours (except $NUV - i$). However, the error contribution is substantial, because age has fairly large uncertainty, compared to its range. Using T^2 to incorporate the errors, we account for over 60 per cent of the variance in $FUV - i$, $FUV - NUV$ and $g - i$, but less than half of the variance in $u^* - g$ and $NUV - i$.

The middle row of panels in Fig. 2 show the equivalent correlations with metallicity. These are in the same sense as the age trends: colours which redden with increasing age also redden with increasing metallicity. The coefficients are significant at the $\sim 5\sigma$ level for all colours except $FUV - i$ (2.6σ). Again, measurement errors contribute substantially to the scatter, since errors on Mg/H individually are large. Based on T^2, the metallicity trends and measurement errors account for about 40 per cent of the variance in most colours, though only 20 per cent in $FUV - i$.

Above, we have modelled the colours as a function *either* of age or of metallicity, but these two parameters are not truly independent. In particular, at fixed velocity dispersion or luminosity, older galaxies tend to be more metal poor (e.g. Trager et al. 2000; Smith et al. 2009). This anticorrelation appears to have an intrinsic component, but there is also a contribution from error covariance, due to the 'tilt' of model grids relative to the line strength indices. Regardless of its source, the mutual correlation between age and metallicity makes it difficult to determine, from single-parameter fits, which parameters are responsible for driving the observed colours. Moreover, population synthesis models show that optical colours, at least, are sensitive to both age and metallicity in similar degree. Hence, to disentangle the effects of age and metallicity, we fit two-parameter models of the form $p = a_0 + a_t \log(t_{\rm ssp}/10\,{\rm Gyr}) + a_Z[{\rm Mg/H}]$, to identify an improved predictor of each colour that combines the age and metallicity effects to minimize the scatter.

In the lower panels of Fig. 2, we express this combination as $\log(t_{\rm ssp}/10\,{\rm Gyr}) + S[{\rm Mg/H}]$, where the ratio $S = a_Z/a_t$ differs for each colour. For the optical colours $u^* - g$ and $g - i$, we recover $S = 1.6$–1.8, in agreement with $S = 1.6$ expected from the 'three-halves rule' of Worthey et al. (1994). Note, however, that Worthey's results were derived from the colours *predicted* by population synthesis models with known age and metallicity. Here, we have instead derived this ratio on the basis of *data* for colour, age and metallicity.[3] For the UV colours, we find that $NUV - i$ is more sensitive to

[3] The fact that our SSP parameters were derived via comparison to synthesis models does not make this a circular argument, since only spectroscopic indices were used to fit the ages, with no information about the broad-band colours.

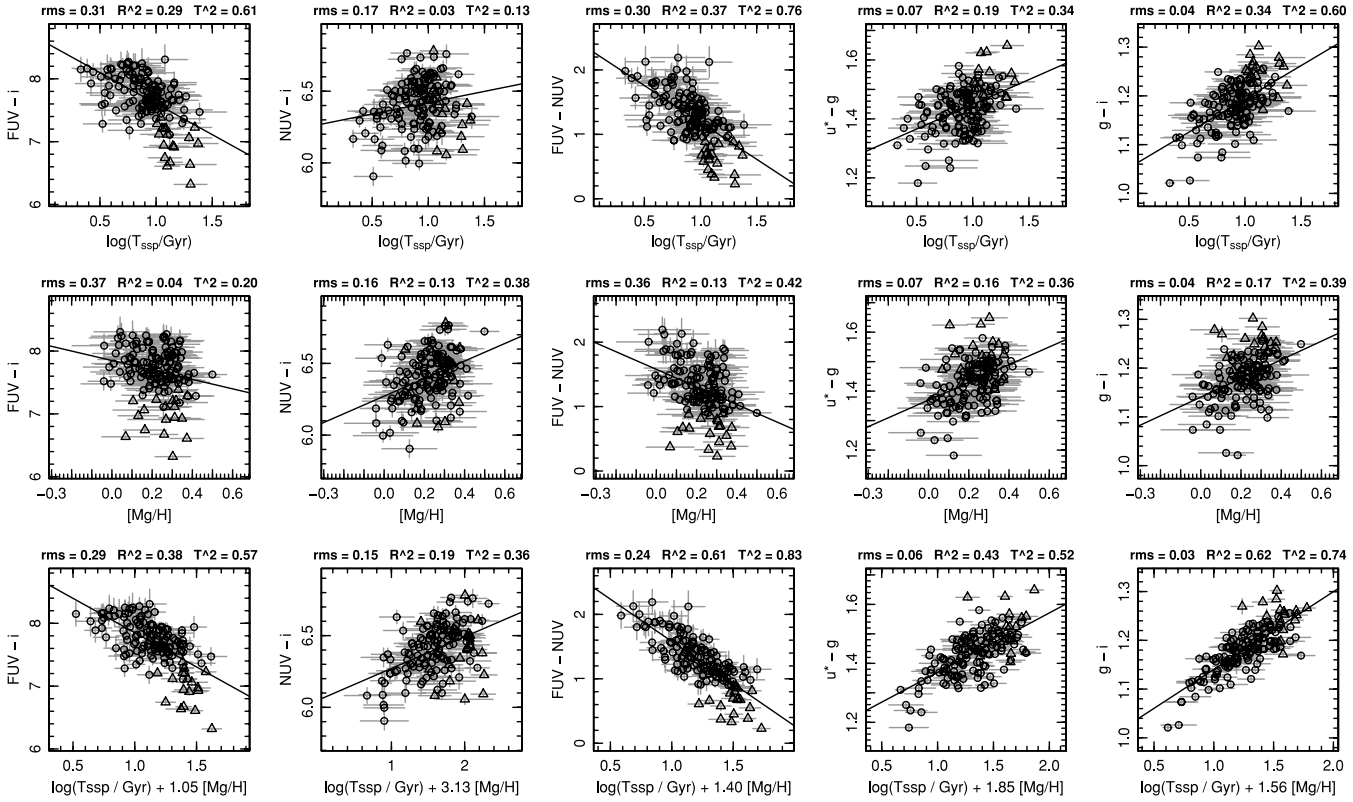

Figure 2. UV and optical colours as a function of age ($T_{\rm SSP}$) and metallicity (Mg/H). The annotations are as in Fig. 1. In the third row, the colours are plotted against the optimal linear combination of age and metallicity, as determined from the simultaneous fits.

Table 4. Comparison of fits using age and Mg/H to those using age and Fe/H. An intercept term has also been fitted but is not reported here.

Colour	Fitting age and Mg/H				Fitting age and Fe/H			
	a_t	a_Z	rms	R^2	a_t	a_Z	rms	R^2
$FUV - i$	-1.092 ± 0.119	-1.144 ± 0.236	0.291	0.38	-1.092 ± 0.159	-0.267 ± 0.250	0.312	0.29
$NUV - i$	$+0.221 \pm 0.062$	$+0.691 \pm 0.124$	0.153	0.19	$+0.488 \pm 0.073$	$+0.845 \pm 0.115$	0.144	0.28
$FUV - NUV$	-1.312 ± 0.097	-1.835 ± 0.192	0.237	0.61	-1.580 ± 0.142	-1.112 ± 0.224	0.279	0.46
$u^* - g$	$+0.202 \pm 0.024$	$+0.373 \pm 0.047$	0.058	0.43	$+0.288 \pm 0.031$	$+0.307 \pm 0.049$	0.062	0.36
$g - i$	$+0.160 \pm 0.012$	$+0.249 \pm 0.023$	0.029	0.62	$+0.225 \pm 0.016$	$+0.225 \pm 0.025$	0.031	0.58

metallicity than to age, compared to the optical colours ($S \approx 3.1$), while $FUV - i$ is somewhat more age sensitive ($S \approx 1.0$). All of the colours studied show significant dependence on both age and metallicity in the simultaneous fits. In Table 4, we compare the fit results obtained if Mg/H is replaced with Fe/H as the metallicity indicator. For most colours, there is little change to the fit results, although the scatter is generally slightly increased when using Fe/H. For $NUV - i$, however, we recover a slightly reduced scatter (marginally significant), and a steeper dependence on age, when using Fe/H. This is likely due to strong line blanketing in the NUV region, which is thought to be dominated by iron lines (Peterson, Dorman & Rood 2001).

Fig. 3 presents these trends in an alternative manner, as maps of average galaxy colour in the age–metallicity plane. The slope of the contours in the maps reflects the relative sensitivity of each colour to age and metallicity. The map for $NUV - i$ appears to show distorted contours indicating a more complex behaviour for this colour. We argue in Section 4.3 that this is due to 'contamination' of the NUV by the old hot stars responsible for the UV upturn.

In most cases, the simultaneous fit to age and metallicity accounts for substantially more of the total variance in colour than either parameter individually, and the residual scatter is comparable to that around the colour–σ relations. The effect of measurement errors is smaller than for the age or metallicity taken separately, because the age errors are anticorrelated with the metallicity errors, and so tend to compensate in the predicted colours.

3.4 Systematics

In this section, we consider possible systematic error sources, and test whether they can make significant contributions to the residual scatter around the fits.

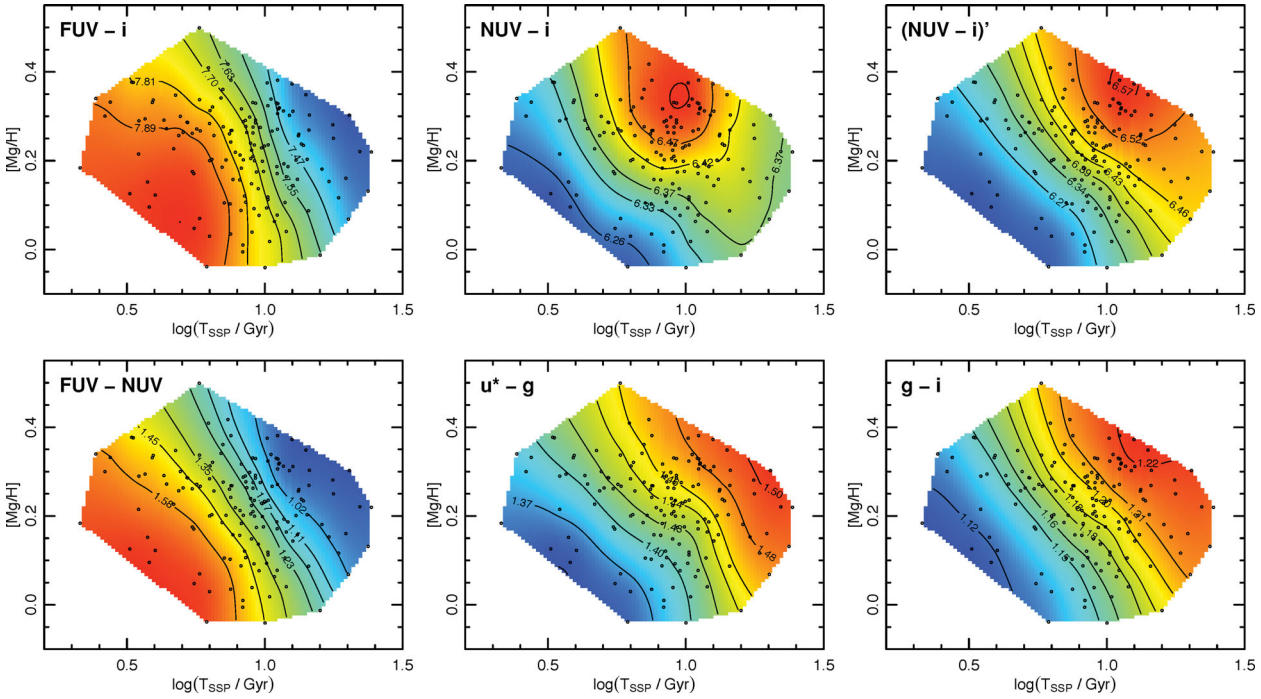

Figure 3. Maps of the average galaxy colour as a function of age and metallicity, created with a Kriging model (e.g. Cressie 1993). The black points indicate the galaxies used to generate the maps. The contours are located at deciles of the colour distribution. The upper right-hand panel shows the results for *NUV* − *i* after correcting for UV-upturn 'leakage' in the *NUV* band (see Section 4.3).

3.4.1 Calibration uncertainties

The aperture magnitude errors adopted for the analysis in Section 3.3 do not include contributions from systematic calibration uncertainties, because most galaxies in the sample are drawn from only a small number of observations (*GALEX* tiles, SDSS drift-scan 'runs', MegaCam pointings). Hence, calibration errors are likely to affect large sections of the data set coherently, rather than on a galaxy-by-galaxy basis. In this section, we assess the evidence for constant shifts between individual 'observations', and their impact on the colour scatter, by allowing additional offset terms in the fits.

For the $g - i$ colour, where SDSS is the only data source, ∼90 per cent of the galaxies were observed in only two drift-scan runs (numbers 5115 and 5087). Including a term representing offsets between runs, we find that colours measured from run 5087 are on average bluer by 0.009 ± 0.005 mag than those measured from run 5115, at similar age and Mg/H. This is consistent with the claimed calibration errors of 0.01 mag in *g* and *i* (Padmanabhan et al. 2008). Although this term is marginally significant, its inclusion does not reduce the residual scatter around the $g - i$ fit, which remains 0.029 mag. A similar test allowing offsets at the level of SDSS camera columns *within* each run does not reveal any further significant systematic effects at above the ∼0.01 mag level.

To test for calibration shifts in the UV versus optical colours, we fit a similar offset term for each *GALEX* tile. Here ∼80 per cent of the galaxies are drawn from two tiles (GI5_025001_COMA and GI2_046001_COMA3). The offset terms are not significant: GI2_046001_COMA3 yields colours on average bluer by 0.04 ± 0.06 mag in *FUV* − *i* and redder by 0.01 ± 0.03 mag in *NUV* − *i*, for galaxies of similar age and metallicity. Again, these limits are consistent with the nominal *GALEX* calibration uncertainties of 0.05 mag (FUV) and 0.03 mag (NUV) quoted by Morrissey et al. (2007). Allowing offset terms does not reduce the residual scatter.

Applying a similar approach to the $u^* - g$ colours reveals that significant systematic errors are present in the MegaCam photometry. Allowing offset terms associated with each of the nine MegaCam pointings, we find that the pointing covering the south-west of Coma (contributing 12 per cent of the sample galaxies) yields colours 0.09 ± 0.01 bluer in $u^* - g$ than the central pointing (57 per cent of the sample), for galaxies of similar age and metallicity. That this is due to calibration errors in MegaCam, rather than SDSS, is confirmed by null results obtained fitting SDSS run offsets (as for $g - i$), either separately, or in combination with MegaCam pointing offsets. The possibility that the offset in the south-west MegaCam pointing is 'astrophysical' rather than systematic can be rejected, given that no corresponding shifts are seen for south-west-region galaxies in residuals for the other colours ($g - i$, *NUV* − *i*, etc.). Allowing for MegaCam offsets reduces the residual scatter in $u^* - g$ from 0.058 to 0.049 mag and the explained fraction of variance increases to $R^2 = 0.63$ (from 0.44).

3.4.2 k-corrections

We did not apply *k*-corrections to the measured colours, due to the uncertainty in the SEDs, especially in the UV. Instead, for each colour we have tested for contributions due to band-shifting, by explicitly including an extra model term proportional to redshift.

A significant effect (∼5σ level) is recovered only for the $u^* - g$ colour. The redshift dependence of $u^* - g$ is not unexpected, since the red cut-off of the u^* filter is close to the 4000 Å break shifted to the mean recession velocity of Coma. Allowing for this dependence increases the explained fraction of variance in $u^* - g$ by a further 6 per cent. Including both the redshift term and the MegaCam systematics discussed above, the explained fraction of variance reaches $R^2 = 0.69$, even without allowing for random errors.

While marginal (2–3σ) *k*-correction terms are also detected in the residuals for $g - i$ and $FUV - NUV$, they contribute negligibly to the variance (1–3 per cent) in these colours.

3.4.3 Aperture mismatch

Our fits compare colours derived in 10-arcsec-diameter photometric apertures against age and metallicity estimates derived from spectroscopy in much smaller apertures (3 arcsec diameter in most cases). An obvious concern is whether mismatch between these apertures contributes to the scatter. This is a particular concern in the UV, which would be sensitive to any ongoing star formation occurring beyond the spectrograph fibre (e.g. Salim & Rich 2010). As for photometric calibration shifts and *k*-corrections, we can constrain these effects by extending our fit with additional terms relating to aperture mismatch.

Since the *GALEX* resolution does not allow use of smaller apertures, we use the SDSS photometry to define a colour shift $\Delta_{gi} = (g - i)_{10\,\mathrm{arcsec}} - (g - i)_{3\,\mathrm{arcsec}}$. On average, Δ_{gi} is negative, indicating that the sample galaxies are typically bluer in $g - i$ within the photometric aperture than within the spectroscopic aperture. This is the sense expected from metallicity gradients in purely passive galaxies.

We constrain the effect of aperture mismatch in our fits by including an additional term proportional to Δ_{gi}. For $FUV - i$, the recovered coefficient is not statistically significant, at -3.1 ± 2.1. The negative coefficient indicates that galaxies that are bluer in the photometric aperture than in the fibre in $g - i$ are globally *redder* in $FUV - i$ than average for galaxies of similar age and metallicity. This is *opposite* to the sense expected if the $FUV - i$ colour scatter were dominated by star formation beyond the spectroscopic fibre. Including the Δ_{gi} term in fit has negligible impact on the residual scatter which remains 0.29 mag. For $NUV - i$, the recovered coefficient is positive but not significant ($+1.4 \pm 1.1$), and its inclusion does not reduce the scatter around the fit, which remains 0.15 mag. For the optical colours, there is a small positive correlation with Δ_{gi}, with no associated reduction in scatter, similar to the case for $NUV - i$. Repeating these tests using colour shift in $u^* - g$ (i.e. Δ_{ug} instead of Δ_{gi}) as an indicator of aperture mismatch yields no further evidence for star formation beyond the fibre aperture, nor any non-negligible reduction in scatter around the fits.

We conclude that unidentified star formation beyond the spectrograph fibre contributes negligibly to the observed colour scatter at fixed age and metallicity.

3.4.4 Internal extinction

Although we cannot exclude the possibility that variations in internal extinction impose some additional scatter in the relationships, it is clear that this does not dominate the residuals. For example, the residual scatter of 0.15 mag in $NUV - i$, if attributed wholly to extinction, would imply a minimum rms of 0.038 mag in $g - i$, which is far in excess of the 0.029 mag observed residual scatter.[4] Moreover, the residuals in $FUV - i$ are anticorrelated with those in $g - i$: galaxies that are redder than average (for their age and metallicity) in the optical are unexpectedly blue in $FUV - i$. Such a relationship cannot be generated only by internal extinction variations. Finally, the distribution of the UV versus optical colour residuals is skewed, with a tail of galaxies extending towards bluer colours. This could be caused only by these galaxies having unusually *low* dust content relative to the average, while the dispersion of internal extinction about its average value remains small. We consider this unlikely.

[4] This calculation assumes the Cardelli, Clayton & Mathis (1989) $R_V = 3.1$ extinction law.

3.4.5 Summary

In summary, having reviewed the likely sources of systematic errors, we find evidence for substantial effects only in the $u^* - g$ colours, due to photometric offsets and band-shifting with redshift. Including these systematic errors, the correlations with spectroscopic age and metallicity account for 70–80 per cent of the variance in the optical colours and in $FUV - NUV$, but still only 40–60 per cent of the variance in $FUV - i$ and $NUV - i$.

3.5 Residual correlations with abundance ratios

We have shown that, using the measured ages and metallicities, we are able to predict optical/UV colours of passive galaxies with the same level of precision as using the velocity dispersion. This suggests that the trends of *mean* colour with σ are adequately reproduced by the trends of *mean* spectroscopic age and metallicity with σ. However, for $FUV - i$ and $NUV - i$, where much of the scatter in colour was unexplained by correlation with velocity dispersion, this scatter was not reduced by using models based on the spectroscopic constraints.

Since element abundances in red-sequence galaxies cannot be adequately described by a single overall metallicity (e.g. Worthey 1998), the abundance ratios of individual elements are obvious candidates for additional parameters which might contribute to driving the colours. In the case of the UV upturn, in particular, the correlation of *FUV* versus optical colours with magnesium line strength indices, and the relative weakness of the correlation with iron-dominated indices, has led many authors to speculate that the UV upturn depends primarily on α-element abundance (O'Connell 1999; B11; Carter et al. 2011).

We have tested for correlations with the element abundances via linear fits of the colour residuals (from the age–metallicity models) against the ratios Fe/Mg, Ca/Mg, C/Mg and N/Mg. (We express all the ratios relative to Mg, rather than the more usual Fe, since we have adopted Mg/H as our overall metallicity indicator.) We fit simultaneously to all the ratios, to disentangle more cleanly the effects of individual elements. The results are summarized in Table 5.

We find only marginal correlations of colours with abundance ratios in most cases. For the Fe/Mg ratio, we find that the $FUV - i$ colour reddens by 0.07 mag, and $FUV - NUV$ reddens by 0.05 mag, for a 0.1 dex increase in Fe/Mg at fixed age and Mg/H (i.e. bluer UV versus optical colours for Mg-enhanced populations). However, these correlations are only $\sim 2.5\sigma$ effects.

Among the other residual trends with abundance ratios, the only significant correlations are for C/Mg: a 0.1 dex enhancement in this ratio (at fixed age and Mg/H) is associated with a 0.01 mag reddening of $g - i$, a 0.03 mag redenning in $NUV - i$ and a 0.06 mag shift bluewards in $FUV - NUV$ (all at 3–4σ). These residual trends are shown in the first two panels of Fig. 4.

To test the robustness of these results, we have also used an alternative approach in which individual abundance ratio terms are incorporated into the fit for each colour as extra parameters, in addition to age and metallicity. Including only Fe/Mg as a third

Table 5. Residual correlations with abundance ratios. Note that because these are fits to the *residuals* from the age–metallicity fits, the coefficients describe the effects of the given abundance ratio at fixed Mg/H. Coefficients that are significant at the $>3\sigma$ level are highlighted with bold-type. The final columns show the small reduction in total scatter when the abundance ratio trends are included in the fit.

Colour residual	[Fe/Mg]	[C/Mg]	[N/Mg]	[Ca/Mg]	Original rms	New rms
$\Delta(FUV-i)$	$+0.67\pm0.26$	-0.33 ± 0.20	-0.12 ± 0.18	-0.15 ± 0.30	0.291	0.284
$\Delta(NUV-i)$	$+0.22\pm0.13$	$\mathbf{+0.30\pm0.10}$	$+0.23\pm0.09$	$+0.00\pm0.15$	0.153	0.141
$\Delta(FUV-NUV)$	$+0.46\pm0.21$	$\mathbf{-0.63\pm0.16}$	-0.36 ± 0.14	-0.15 ± 0.23	0.237	0.222
$\Delta(u^*-g)$	$+0.02\pm0.05$	$+0.10\pm0.04$	$+0.07\pm0.04$	-0.02 ± 0.06	0.058	0.056
$\Delta(g-i)$	$+0.00\pm0.02$	$\mathbf{+0.10\pm0.02}$	$+0.04\pm0.02$	$+0.01\pm0.03$	0.029	0.025

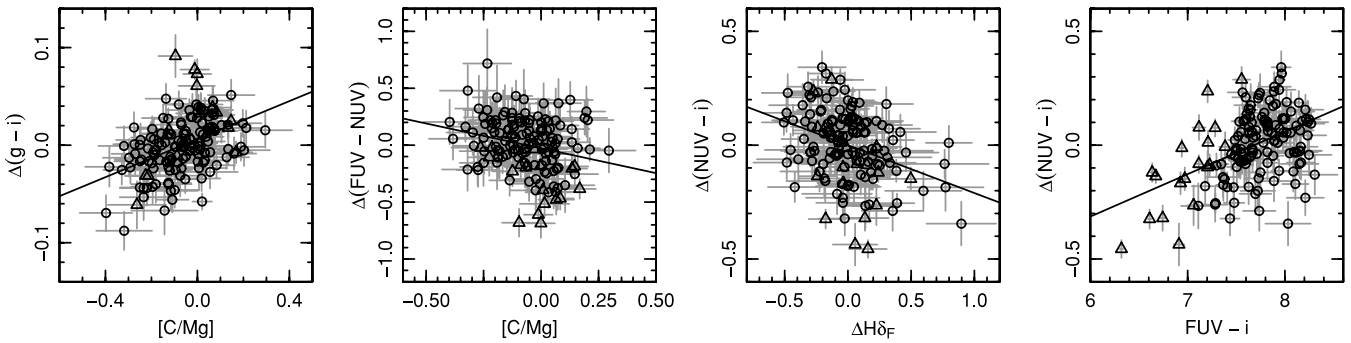

Figure 4. Residual correlations discussed in the text. The residuals $\Delta(NUV-i)$, etc., are as measured from the fits using age and metallicity simultaneously to predict the colours. The vertical error bars include the errors in the predictor variables, corrected for covariance as necessary.

parameter, we find significant trends for $FUV-i$ ($+0.80\pm0.30$), $NUV-i$ ($+0.69\pm0.16$) and $g-i$ ($+0.11\pm0.03$). Repeating this test with C/Mg as a third parameter instead of Fe/Mg, significant trends are found for $NUV-i$ ($+0.33\pm0.09$), $FUV-NUV$ (-0.45 ± 0.15) and $g-i$ ($+0.10\pm0.02$). For u^*-g, a significant trend with C/Mg ($+0.16\pm0.03$) is recovered after accounting for the systematic effects noted in Section 3.4. These results are qualitatively similar to those obtained from the simultaneous fit to the residuals, although individual coefficients are sensitive to the fitting treatment adopted.

To summarize, decoupling the effects of multiple abundance ratio parameters, in addition to the age and metallicity trends, remains difficult. The strongest abundance ratio effects in the UV seem to be related to Fe/Mg and C/Mg, with little dependence on Ca/Mg or N/Mg. The abundance ratio effects make modest contributions to the total observed scatter, increasing R^2 by 8 per cent for $NUV-i$ and $g-i$, and by 4–6 per cent in $FUV-i$, $FUV-NUV$ and u^*-g.

4 DISCUSSION

4.1 The index versus colour relations reconsidered

As reviewed in the Introduction, early work revealed a strong correlation between the FUV versus optical colour and the Mg_2 line index (Burstein et al. 1988), from which it was inferred that the FUV output of passive galaxies depends mainly on metallicity. Equivalent conclusions were drawn by B11, using much improved data, from the strong correlation of the Mg*b* index with the $FUV-V$ colour. In this section, we address the apparent disagreement between this view and the results of our analysis which instead favour a dominant age dependence of the FUV versus optical colour, and only a weaker residual trend with metallicity. We base our argument on comparison with B11, but qualitatively the same case applies to Burstein et al. (1988) and other studies following a similar analysis approach.

In Fig. 5, we show the correlations of $FUV-g$ (to match B11's $FUV-V$) with the Mg*b* and Hβ line strength indices. As before, we treat *colour* as a dependent variable, and fit the relations by minimizing scatter in the colour direction. For comparison we show also the fits quoted by B11. Their approach minimizes scatter in the *line strength* direction and their fits are made only to galaxies with H$\beta<1.8$ Å. To account for the different colour definitions used, the B11 fits have been shifted to pass through the average position of our H$\beta<1.8$ Å galaxies, but the slopes are as quoted in their paper. As always for correlations with substantial scatter, the fits differ significantly according to the direction of minimization. Fitting our data in the same way as B11 fit theirs, we would recover similar slopes. Hence at the level of the data, our index versus colour correlations are consistent with earlier work.

The origin of the different conclusions we reach, with respect to B11, lies in three differences in our analysis: the choice of minimization direction, the treatment of the high-Hβ data points and the interpretation of the recovered trends.

Minimizing in the colour direction implies asking which parameters are the best *predictors* of colour. When considering age and metallicity as predictors (as in Section 3.3), there are strong grounds for assuming a causal relationship, since these parameters at least in part determine the stellar content, and hence the broad-band colours. However, even individual line strength indices are related to the properties of the optically-dominant stellar population in a fairly direct way. The UV colours by contrast have long appeared to exhibit large scatter with respect to all of the optical properties. Hence, colour is the quantity with 'unknown' behaviour, and consequently we prefer to treat it as a dependent variable.

The effect of excluding strong-Hβ (i.e. young and/or metal-poor) galaxies itself depends on the minimization direction. Minimizing residuals in colour, as in our approach, the derived trend is

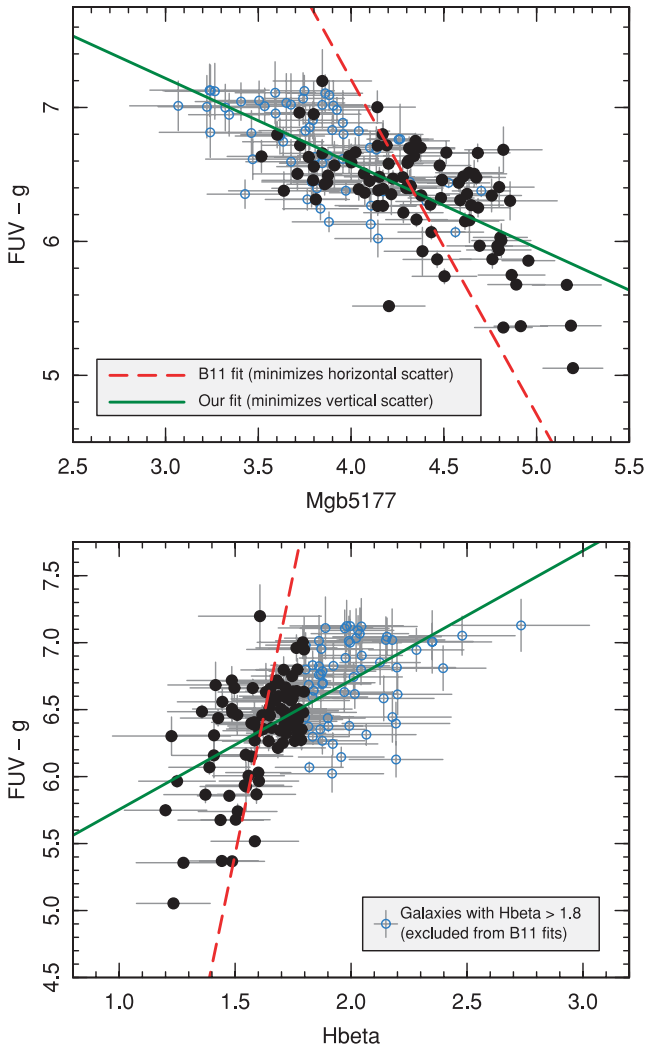

Figure 5. The line strength versus colour relations, for comparison to previous work, in particular B11. The green line shows our fit to the Coma data, minimizing in the colour direction, as throughout our work. The red line shows the B11 fits (to their data), which minimize in the line strength direction and exclude galaxies with Hβ > 1.8 Å.

unchanged by such a cut, to first order, even when fitting Hβ itself. By contrast, if we minimize residuals in index strength (as done by B11), the resulting fit is highly biased for Hβ, since all Hβ values are included at blue colours, but only unrepresentatively low Hβ values contribute at redder colours. The bias is less strong for Mg*b*, since the selection is not in the fitted quantity, but still present because Mg*b* tends to be anticorrelated with Hβ. (Note that our fits may be slightly affected by a bias in the opposite sense: since our sample is limited by magnitude error in the FUV, the reddest galaxies may be preferentially excluded at the faint end.)

Thus, we can understand why the different choice of fit direction and exclusion of strong-Hβ galaxies led B11 to a steeper slope for the colour versus Mg*b* relation (inverting the values in their table 2 gives $-2.5^{+0.5}_{-0.7}$ mag Å^{-1} compared to our slope of -0.63 ± 0.05 mag Å^{-1}) and a dramatically steeper slope for the colour versus Hβ relation ($+8.3^{+5.9}_{-2.5}$ mag Å^{-1} compared to our $+0.97 \pm 0.10$ mag Å^{-1}). It might be expected, then, that B11 would infer a much steeper age dependence for the FUV versus optical colour than we do. Instead, they imply that the trend results from the known dependence of Hβ on metallicity, and hence that a correlation between FUV and metallicity drives both the colour–Mg*b* and colour–Hβ relationships. B11 do acknowledge that the high-Hβ outliers from their fits are driven by younger ages. Our interpretation of their results is that these 'outliers' in fact fall along the more meaningful correlation obtained by fitting the full data set.

In summary, the conclusions reached in our work disagree with those of B11 mainly through our preferred approaches for fitting and interpreting the data.

4.2 The origin of the FUV upturn

One motivation for this work was to explore the age and metallicity dependence of the FUV upturn, as a method to distinguish between the 'metal-rich single-star hypothesis' (e.g. Yi et al. 1997b) and the 'binary-star hypothesis' (Han et al. 2007) for the origin of the FUV flux in passive galaxies. Although only ∼13 per cent of galaxies in our sample have classic FUV upturns, in the sense of having rising f_λ versus λ below 2000 Å ($FUV - NUV < 0.9$), we prefer a 'continuous' treatment of the colours, rather than imposing a discrete classification as done, for instance, by Yi et al. (2011).

In both the Han et al. and Yi et al. models, the FUV upturn is caused by helium-burning stars with very thin hydrogen envelopes, having effective temperatures ∼25 000 K. In addition to this EHB[5] phase itself, the subsequent post-HB evolution of such stars can include long-lived UV-luminous phases (e.g. the failed asymptotic giant branch, or AGB-Manqué). These stars were identified as probable sources of the UV upturn through their good match to the spectra (both continuum and lines) of strong-upturn galaxies like NGC 1399 (e.g. Ferguson et al. 1991). *Hubble Space Telescope* (*HST*) imaging of M32 by Brown et al. (2000, 2008) has confirmed the presence of EHB and post-EHB stars, and their dominance of the FUV emission in this (weak-upturn) elliptical.

The Han et al. and Yi et al. models differ in the channels by which stars reach the EHB, and hence in their dependence on age and metallicity. In the single-star model, Yi et al. (following Greggio & Renzini 1990) postulate EHB formation through an enhanced efficiency of mass loss on the RGB at high metallicity, leading to low envelope mass and high temperature on the HB. The evolution of such stars after they leave the HB is also sensitive to envelope mass, and hence to metallicity, with a larger fraction of high-metallicity stars following the UV-luminous AGB-Manqué pathway instead of evolving on to the AGB. Finally, there is a strong age dependence because stars of smaller initial mass need to lose less mass to reach the EHB and the UV-bright post-HB phases. In the models favoured by Yi, Demarque & Oemler (1997b, their fig. 16), the envelope-mass threshold governing the post-HB evolution causes an extremely rapid onset of the UV upturn, for example, a 2–4 mag boost in FUV between ages of 10 and 15 Gyr. For younger ages the evolution is much slower, perhaps equivalent to a slope of 0.3–0.6 mag per decade in age. The effect of metallicity is primarily to affect the age at which the rapid UV boost occurs, such that metallicity trends at constant age may be very strong or very weak, depending on the age range considered.

In the Han et al. scenario, EHB stars form through a variety of binary interactions, including stable Roche lobe overflow, common-envelope evolution and mergers of binary white dwarfs. In these models, the FUV versus optical colours are only weakly dependent

[5] Han et al. (2007) refer to these stars more generally as hot subdwarfs, since they consider a wide range in formation mechanisms.

on age for an SSP. For example, from table 2 of Han et al. (2007), fitting the $FUV - r$ colour over a range of 3–12 Gyr, we obtain a slope of −0.3 mag per decade in age. The influence of metallicity is not fully addressed: although channels for the formation of EHB stars are not thought to depend on metallicity, their subsequent evolution may do so, and this is not followed in the model.

In testing the observed age and metallicity dependence of the upturn, we note that the proposed correlations are 'indirect': the hot stars responsible for the FUV excess are too faint at optical wavelengths to contribute substantially to the spectroscopic indices. Rather, we are testing the hypothesis that (a) the mechanisms for *producing* these stars are affected by the age and metallicity of the stellar population from which they evolved, and (b) that this population was either the same as, or at least correlated with, the stellar population which today dominates the optical spectrum.

We adopt the observational results for $FUV - i$ as the most direct tracer of the upturn population (see Section 4.4 for comments on $FUV - NUV$). The fits presented in Section 3.3 suggest that $FUV - i$ is primarily sensitive to age, becoming bluer for older galaxies with a slope of 1.1 ± 0.1 mag per decade in age. At fixed age, there is also a dependence on metallicity, such that $FUV - i$ becomes bluer by 1.1 ± 0.2 mag per decade increase in Mg/H. The sense of the observed age trend is as predicted by both the Han et al. and Yi et al. models, but its slope is much steeper than predicted by Han et al. As noted above, the age dependence in Yi et al. is non-linear, becoming extremely steep at ages above 10 Gyr. Some steepening is evident in the upper left-hand panel of Fig. 2 as an increased scatter on the blue side of the distribution at ages above ∼10 Gyr. Quantifying this by splitting the sample at the median age of 9 Gyr, we find that the older galaxies show a slope of 1.5 ± 0.3 per decade in age, while the younger galaxies have only a marginal dependence of 0.5 ± 0.2 per decade. This behaviour is difficult to reconcile with the Han et al. model, but is a generic prediction of the Yi et al. scenario. We note that a strong dependence at the oldest ages is also suggested by the apparently rapid redshift evolution of the UV upturn (e.g. Brown et al. 2003; Ree et al. 2007, but see also Atlee, Assef & Kochanek 2009). The Yi et al. model also predicts that the FUV-to-optical colour becomes bluer with increasing metallicity, but the strength of the metallicity effect itself depends on age. Based on fig. 16 of Yi et al. (1997b), we would expect a trend of the order of 10 mag per decade in Mg/H for galaxies with ages of 15 Gyr, but only ∼0.8 mag per decade at 5–10 Gyr ages. The latter is broadly consistent with the trend derived from our fits.

Despite recovering a strong age dependence in the $FUV - i$ colour, we continue to find a large scatter around the average trend, with variations in the optically-dominant stellar populations accounting for only ∼39 per cent of the total variance in colour, and a further 19 per cent is contributed by measurement error. There are only marginal correlations of $FUV - i$ with element abundance ratios, which do not substantially reduce the scatter. Hence, a simple, deterministic, explanation of the FUV colours appears inconsistent with SSP models, at least to the extent that they can be constrained from the optical spectra. Considering more realistic extended star formation histories (SFHs), in combination with the threshold age effect in the Yi et al. models, perhaps offers a more promising explanation for the scatter in $FUV - i$. The SSP-equivalent age is essentially a weighted average over the true distribution of stellar ages. Because in the Yi et al. scenario the oldest populations produce dramatically more FUV flux, the $FUV - i$ colours for a galaxy with extended SFH will be sensitive to the fraction of stars in the old tail of the age distribution. As a simplified example, consider a case where populations older than 12 Gyr receive an instantaneous 2 mag boost to their FUV flux. A galaxy with Gaussian SFH with mean age $t_0 = 10$ Gyr and dispersion $\sigma_t = 1$ Gyr has 2.3 per cent of its stellar content FUV-boosted, resulting in a total flux 0.12 mag brighter in FUV than an SSP of the same age. Keeping the same mean age, but increasing the dispersion to $\sigma_t = 1.5$ Gyr, results in boosting ∼9.1 per cent of the stellar content, increasing the total flux by a *further* 0.31 mag.[6] Thus, if the FUV luminosity increase for the oldest galaxies is sufficiently strong and rapid, then the observed excess scatter of ∼0.3 in $FUV - i$ could be attributable to a modest variation in star formation time-scale, at a given mean age.[7] Further investigation is required to test whether this explanation is viable, given more realistic and detailed models of the flux evolution.

In conclusion, the observed relationship between the $FUV - i$ colour and spectroscopic age and metallicity appears to favour the metal-rich single-star EHB hypothesis for the origin of the UV upturn. This scenario generically predicts a dependence on age in particular among the oldest galaxies, and on metallicity. The large scatter at given SSP-equivalent age and metallicity can possibly be explained through galaxy-to-galaxy variations in early SFH. The binary hypothesis cannot account naturally for these results.

4.3 Excess scatter at the NUV: residual star formation or UV-upturn leakage?

A second motivation for our study was to investigate the cause of the large scatter seen in NUV versus optical colours.

The NUV to optical scatter has been interpreted as evidence for recent or widespread ongoing star formation in optically-red galaxies (e.g. Kaviraj et al. 2007). A sample definition is critically important to this result, since objects with *ongoing* star formation will evidently have blue UV colours. For our analysis, we excluded galaxies with central Hα emission from the spectroscopy. The remaining objects have only ∼0.16 mag scatter around the $NUV - i$ colour–magnitude (or colour−σ) relation, compared to values in the range 0.3–0.6 mag reported in the literature (Boselli et al. 2005; Yi et al. 2005; Haines, Gargiulo & Merluzzi 2008; Rawle et al. 2008). Star formation occurring further from the nucleus cannot be excluded, but does not appear to dominate the colour scatter (Section 3.4.3).

We now consider the correlations of $NUV - i$ with spectroscopic age and metallicity. Unlike in the FUV case we are here testing 'direct' correlations, in the sense that the *same* stars (in particular warm main-sequence turn-off stars) are expected to contribute to the NUV colour variations and to the spectroscopic ages. We find significant trends for bluer colours at lower metallicity (the dominant effect, as found also by Rawle et al. 2008) and at younger age. While the age dependence is qualitatively as expected from evolutionary synthesis models, the slopes that we obtain from the fits (e.g. ∼0.2 mag per decade in age) are much shallower than the predictions derived by Dorman, O'Connell & Rood (2003), who report a 2–3 mag change in $NUV - V$ per decade in age. The evolution of $NUV - i$ in the Bruzual & Charlot (2003) models is more gradual, with ∼0.65 mag change per decade in age, though still steeper than our measured

[6] In general, for a Gaussian SFH with mean age t_0, age dispersion σ_t, and a flux-boost factor b imposed on ages above T, the total flux is increased by a factor $f = \frac{1}{2}(1+b) + \frac{1}{2}(1-b)\,\mathrm{erf}\left(\frac{T-t_0}{\sqrt{2}\sigma_t}\right)$.

[7] However, if the α element abundance ratio is interpreted as a star formation time-scale indicator (Thomas et al. 2005), then this explanation also predicts that bluer $FUV - i$ (at given age) would be accompanied by higher Fe/Mg ratios, contrary to the observed trend.

trends. (The Bruzual & Charlot models do not include blue HB stars; their presence would further dilute the predicted age trend.)

Age and metallicity variations account for only 20 per cent of the total variation in $NUV - i$, leaving a residual scatter of 0.15 mag around the fit. Splitting the sample by spectroscopic age, we find that the fit is poorer (i.e. larger scatter and smaller R^2) for the *oldest* galaxies in the sample. For galaxies older than the median age of 9 Gyr, the age and metallicity effects account for only 12 per cent of the variance. For galaxies younger than 9 Gyr, correlations with age and Mg/H jointly account for 44 per cent of the total variance.

As noted elsewhere, the SSP equivalent is only a weighted average over the unknown true SFH of the galaxy. For example, an SSP age of ∼5 Gyr may represent a population formed mostly at early epochs, but with a small mass fraction added in the past ∼Gyr. We have tested whether the remaining scatter in $NUV - i$ is due to young subpopulations, using the Hδ_F index. Discrepancies in Hδ_F compared to the (Hβ-based) SSP-equivalent age estimates can be interpreted as evidence for star formation within the past ∼2.5 Gyr (Serra & Trager 2007), or alternatively as evidence for contributions from other warm stars, for example, on the blue HB (Schiavon et al. 2004). We consider the residuals from the fit of $NUV - i$ versus age and metallicity, and compare them to the residuals from a fit of Hδ_F against age and metallicity (third panel of Fig. 4). The residuals from the two fits are anticorrelated, as expected: galaxies with stronger Hδ_F than expected from their SSP-equivalent ages and metallicity are also bluer than the average galaxy at that age and metallicity. The correlation is significant at the $\sim 4\sigma$ level, and this dependence accounts for ∼8 per cent of the total variance in $NUV - i$. Thus, variations in true SFH (or blue HB content), as traced by Hδ_F, make a measurable, but minor, contribution to the remaining $NUV - i$ scatter at a given SSP-equivalent age and metallicity. (Equivalent tests for the other colours reveal 2–3σ trends for $u^* - g$ and $g - i$, which is $\lesssim$3 per cent to the variance in these colours.)

The above results suggest that the excess scatter at the NUV is related to old populations, rather than to young stars. We hence explore here whether $NUV - i$ is significantly affected by the old helium-burning stars, that is, the UV-upturn sources. The possibility that such sources make a significant contribution to the flux at the NUV has previously been discussed in previous work (e.g. Dorman et al. 2003; Rawle et al. 2008). If we adopt $FUV - i$ as an indicator for the strength of the upturn population, we find that $\Delta(NUV - i)$, defined as the residual from the age–metallicity fit for this colour, is correlated with $FUV - i$ at the 6σ level (fourth panel of Fig. 4). (By contrast the $NUV - i$ colour itself shows only an $\sim 2\sigma$ correlation with $FUV - i$, because other factors *are* important in driving the NUV flux.) This result suggests that some of the excess scatter in the fits to $NUV - i$ results from 'leakage' of the FUV upturn. Incorporating $FUV - i$ as an additional term in a simultaneous fit for $NUV - i$ reduces the scatter from 0.15 to 0.13 mag. In the resulting fit, the coefficient of $FUV - i$ is 0.31 ± 0.04; the slope with $\log T_{\rm ssp}$ is increased to ∼0.55 (in better agreement with the Bruzual & Charlot models), and that of [Mg/H] is increased to ∼1.0. The resulting coefficient of determination is increased from $R^2 = 0.20$ to 0.48. The effect of 'correcting' $NUV - i$ for the FUV leakage can be seen in the upper right-hand panel of Fig. 3. Comparison to the equivalent panel for uncorrected $NUV - i$ shows that the correction makes the oldest galaxies redder (since these are the galaxies with strongest UV upturn) and hence yields a map similar in form to the optical colours. It has been suggested that the FUV-upturn sources may even affect the 'optical' U band (e.g. Yi et al. 1997b). However, we find no correlation of the $u^* - g$ (or $u^* - i$) residuals with $FUV - i$, equivalent to the trends seen at the NUV. We infer that 'leakage' of the upturn does not extend significantly to the fairly red u^* bandpass used in our MegaCam observations.

Thus, whatever the sources of the FUV variation might be, they are likely to cause a significant fraction of the scatter observed in the NUV as well. Of course, this result does not, on its own, prove that the correlated excess variation in the FUV and NUV are both due to old hot stars (i.e. the classic UV upturn population), rather than both being due to residual ongoing star formation. We consider the latter possibility unlikely though, because on other grounds it is clear that the UV upturn itself is *in general* not due to young stars (O'Connell 1999, and references therein). Moreover, recall that $FUV - i$ is bluer for older spectroscopic age. If ongoing star formation were responsible for variations in $FUV - i$, it would have to occur preferentially in galaxies that have *not* formed stars at the intermediate ages (∼1 Gyr) which strongly affect the SSP fits.

Finally, we note that Salim & Rich (2010) have presented *HST* FUV imaging revealing clear signatures of star formation in a sample of 'quiescent early-type galaxies' that have no detectable Hα in SDSS.[8] The Salim & Rich sample, however, was constructed explicitly to select galaxies that are *unusually* blue in $FUV - i$, relative to their other properties, so that by definition they are outliers from the overall population. Indeed, almost all of their sample galaxies are much bluer, in both $FUV - i$ and $NUV - i$, than any of our Coma galaxies (measured relative to the peak of the red sequence in the respective studies). Although their result confirms that nuclear Hα measurements alone cannot exclude all star-forming galaxies, it does not imply that such galaxies are common among samples selected to be *representative* of the optical red/passive sequence.

We conclude that a majority of the observed scatter in the NUV versus optical colour can be adequately accounted for by a combination of (i) variation in age and metallicity as inferred from optical spectroscopy (∼20 per cent of total variance), (ii) a significant contribution from the same old hot stars which dominate the FUV scatter (∼30 per cent), (iii) a minor contribution from abundance ratio effects and variation in SFH at given SSP-equivalent age (∼15 per cent), and (iv) measurement error (∼15 per cent). There is little need to invoke widespread 'residual star formation' to explain the NUV colour scatter in our sample.

4.4 A comment on the tight correlations for $FUV - NUV$

We have shown that the overall strength of the UV upturn, as traced by $FUV - i$, shows scatter that cannot be accounted for by variations in the optically-dominant stellar populations. However, the $FUV - NUV$ colour is surprisingly well behaved, in the sense that most of its variation is predictable from the velocity dispersion, or from age and metallicity, with a precision similar to that found for the optical colours. (This statement is in fact equivalent to our conclusion that leakage from the UV upturn contributes much of the excess scatter in $NUV - i$.) Age and metallicity variations account for ∼60 per cent of the total variance in $FUV - NUV$, with a further ∼20 per cent attributable to measurement errors.

That the $FUV - NUV$ colour follows tighter relations than the FUV versus optical colours has been noted before (Donas et al. 2007), and B11 conclude that $FUV - NUV$ should be the preferred colour to investigate the UV upturn. We disagree with this position: given the consensus that the upturn sources are hot old stars, the

[8] Although in fact half of the examples they show are evidently spirals on the basis of the SDSS imaging alone.

crucial quantity is their *incidence* relative to cool stars of similar age, which is best traced using the red-optical or near-IR flux.

Simplistically, the $FUV - NUV$ colour should be sensitive instead to the *temperature* of the upturn sources, which would provide further constraints on the origin of the upturn. For instance, fig. 14 of Yi et al. (1997b) shows that within their model, the post-EHB stars generate more FUV flux than the EHB itself, while in the NUV the contributions of EHB and post-EHB stars are comparable. In practice, however, any attempt to extract information from the $FUV - NUV$ colour alone will be confused by its sensitivity to at least three influences: (i) the age and metallicity of the pre-HB stellar population, via the main-sequence turn-off, (ii) the overall strength of the UV-upturn population, and (iii) the spectral slope of the upturn. In particular the strong observed $FUV - NUV$ correlations likely arise from a compounding of effects (i) and (ii): increasing age and metallicity has the effect of suppressing the NUV flux from the main sequence, as well as boosting the FUV flux from the helium-burning populations.

We conclude that the $FUV - NUV$ colour will be of limited use in deciphering the origin of the upturn, unless additional information from longer wavelengths is incorporated.

5 CONCLUSIONS

We have analysed the UV and optical colours of 150 galaxies in the Coma cluster, selected to lie on the (optical) red sequence and to have no detectable Hα emission. Using ages and metallicities derived from optical spectroscopy, we have performed a purely empirical test for the origin of scatter in the colours. Our primary conclusions are as follows:

(i) All of the UV and optical colours we investigate show strong ($>5\sigma$) correlations with luminosity and with velocity dispersion.

(ii) The average trends in galaxy colours as a function of velocity dispersion can be accounted for by their correlation with the spectroscopically measured SSP-equivalent ages and metallicities. $NUV - i$, $u^* - g$ and $g - i$ become redder with increasing age or metallicity, while $FUV - NUV$ and $FUV - i$ become bluer.

(iii) For the optical colours, and for $FUV - NUV$, most (70–80 per cent) of the variance in galaxy colours can be accounted for by correlations with spectroscopic age and metallicity, once random and systematic error sources are included.

(iv) For the $FUV - i$ colour, which traces the UV upturn, a strong anticorrelation with age is observed, combined with an anticorrelation with metallicity. The correlations are in the sense predicted by single-star EHB models for the origin of the FUV flux in passive galaxies (Yi et al. 1997b), and contrary to the weak dependences predicted by the binary hypothesis of Han et al. (2007).

(v) However, only ~60 per cent of the variance can be accounted for, even when measurement errors are included. Moreover, the galaxies with the oldest SSP-equivalent ages (>10 Gyr) apparently show an excess flux in the FUV which is not captured by the linear fits. Such a steepening at high age is predicted by the single-star EHB models. The excess scatter at the FUV could result from a varying contribution from such ancient stars in galaxies with younger SSP ages but extended SFHs.

(vi) Excess scatter is also observed for the colour $NUV - i$. The residuals are highly correlated with the $FUV - i$ colour, suggesting that the stars responsible for the UV upturn also contribute significantly to the scatter in the NUV. Variation in the true extended SFHs, at a given value of the SSP-equivalent age, makes only a small contribution to the $NUV - i$ colour scatter. There is no need to invoke widespread 'residual star formation' to account for the observed NUV scatter in our sample.

(vii) At fixed age and Mg/H, colours are weakly correlated with the Fe/Mg and C/Mg abundance ratios, with no significant dependence on Ca/Mg or N/Mg. Abundance ratio variations, at fixed Mg/H, contribute only modestly to the scatter in the UV colours.

(viii) Combining all effects addressed in this paper, we can account for 80–90 per cent of the scatter in all of the colours studied, except for $FUV - i$. The contributions are summarized in Table 6.

Because we have limited our analysis to empirical correlations, the above results are independent of any specific population synthesis models for the UV colours. The measured correlations and variances should provide a good comparison data set for future model-based investigations.

ACKNOWLEDGMENTS

RJS was supported for this work by STFC Rolling Grant PP/C501568/1 'Extragalactic Astronomy and Cosmology at Durham 2008–2013'. We are grateful to Ann Hornschemeier, Derek Hammer and Tim Rawle for contributions to the *GALEX* proposal

Table 6. Summary of the sources of variance in the colours as determined in this paper. The contributions are expressed as a fraction (in per cent) of the total variance in each colour. We distinguish 'astrophysical' sources of variance, that is, correlations with intrinsic galaxy properties, from those due to systematic errors in the measurements. The sum of these constitutes the total 'structural' component of the variance, that is, the fraction attributable to known dependencies. Adding the variance due to random errors, we arrive at the total fraction of variance that has been accounted for. All components below the ~4 per cent level are omitted for clarity. The most important lines in the table are emphasized in bold text for ease of comparison.

Contribution		$FUV - i$	$NUV - i$	$FUV - NUV$	$u^* - g$	$g - i$	Section
Astrophysical:							
	Age/metallicity	**39**	**20**	**62**	**44**	**63**	3.3
	Abundance ratios	5	8	4	6	8	3.5
	Young subpopulations		8				4.3
	UV-upturn leakage		28				4.3
Systematics:							
	Photometric calibration				19		3.4.1
	k-correction				6		3.4.2
Total structural component		**44**	**64**	**66**	**75**	**72**	
Random errors		19	17	21	9	9	3.1
Total explained component		**63**	**81**	**87**	**83**	**81**	

and comments on drafts of this paper, and to our other collaborators in the Coma Hectospec survey. We thank Zhanwen Han for comments about the binary star models for the UV upturn, and the anonymous referee for numerous helpful suggestions. This work is based on observations made with the National Aeronautics and Space Administration (NASA) *GALEX*. *GALEX* is a NASA Small Explorer, developed in cooperation with the Centre National d'Etudes Spatiales of France and the Korean Ministry of Science and Technology.

Funding for the SDSS and SDSS-II has been provided by the Alfred P. Sloan Foundation, the Participating Institutions, the National Science Foundation, the US Department of Energy, NASA, the Japanese Monbukagakusho, the Max Planck Society, and the Higher Education Funding Council for England. The SDSS website is http://www.sdss.org/. The SDSS is managed by the Astrophysical Research Consortium for the Participating Institutions. The Participating Institutions are the American Museum of Natural History, Astrophysical Institute Potsdam, University of Basel, University of Cambridge, Case Western Reserve University, University of Chicago, Drexel University, Fermilab, the Institute for Advanced Study, the Japan Participation Group, The Johns Hopkins University, the Joint Institute for Nuclear Astrophysics, the Kavli Institute for Particle Astrophysics and Cosmology, the Korean Scientist Group, the Chinese Academy of Sciences (LAMOST), Los Alamos National Laboratory, the Max Planck Institute for Astronomy, the Max Planck Institute for Astrophysics, New Mexico State University, Ohio State University, University of Pittsburgh, University of Portsmouth, Princeton University, the United States Naval Observatory and the University of Washington.

REFERENCES

Atlee D. W., Assef R. J., Kochanek C. S., 2009, ApJ, 694, 1539
Bernardi M., Sheth R. K., Nichol R. C., Schneider D. P., Brinkmann J., 2005, AJ, 129, 61
Bertin E., Arnouts S., 1996, A&AS, 117, 393
Bohlin R. C., Cornett R. H., Hill J. K., Hill R. S., O'Connell R. W., Stecher T. P., 1985, ApJ, 298, L37
Boselli A. et al., 2005, ApJ, 629, L29
Brown T. M., Bowers C. W., Kimble R. A., Sweigart A. V., Ferguson H. C., 2000, ApJ, 532, 308
Brown T. M., Ferguson H. C., Smith E., Bowers C. W., Kimble R. A., Renzini A., Rich R. M., 2003, ApJ, 584, L69
Brown T. M., Smith E., Ferguson H. C., Sweigart A. V., Kimble R. A., Bowers C. W., 2008, ApJ, 682, 319
Bruzual G., Charlot S., 2003, MNRAS, 344, 1000
Bureau M. et al., 2011, MNRAS, 414, 1887 (B11)
Burstein D., Bertola F., Buson L. M., Faber S. M., Lauer T. R., 1988, ApJ, 328, 440
Cardelli J. A., Clayton G. C., Mathis J. S., 1989, ApJ, 345, 245
Carter D., Pass S., Kennedy J., Karick A., Smith R. J., 2011, MNRAS, 414, 3410
Catelan M., 2009, Ap&SS, 320, 261
Chung C., Yoon S.-J., Lee Y.-W., 2011, ApJ, 740, L45
Code A. D., Welch G. A., 1979, ApJ, 228, 95
Cressie N. A. C., 1993, Statistics for Spatial Data. Wiley, New York
Donas J. et al., 2007, ApJS, 173, 597
Dorman B., O'Connell R. W., Rood R. T., 2003, ApJ, 591, 878
Ferguson H. C. et al., 1991, ApJ, 382, L69
Godwin J. G., Metcalfe N., Peach J. V., 1983, MNRAS, 202, 113
Graves G. J., Schiavon R. P., 2008, ApJS, 177, 446
Graves G. J., Faber S. M., Schiavon R. P., 2009, ApJ, 693, 486
Greggio L., Renzini A., 1990, ApJ, 364, 35
Haines C. P., Gargiulo A., Merluzzi P., 2008, 385, 1201
Hammer D., Hornschemeier A. E., Mobasher B., Miller N., Smith R. J., Arnouts S., Milliard B., Jenkins L., 2010, ApJS, 190, 43
Han Z., Podsiadlowski Ph., Lynas-Gray A. E., 2007, MNRAS, 380, 1098
Kaviraj S. et al., 2007, ApJS, 173, 619
Lee H.-c., Yoon S.-J., Lee Y.-W., 2000, AJ, 120, 998
Loubser S. I., Sánchez-Blázquez, 2011, MNRAS, 410, 2679
Magnier E. A., Cuillandre J.-C., 2004, PASP, 116, 449
Maraston C., 2005, MNRAS, 362, 799
Marino A. et al., 2011, MNRAS, 411, 311
Martin D. C. et al., 2005, ApJ, 619, L1
Morrissey P. et al., 2007, ApJS, 173, 682
O'Connell R. W., 1999, ARA&A, 37, 603
O'Connell R. W. et al., 1992, ApJ, 395, L45
Padmanabhan N. et al., 2008, ApJ, 674, 1217
Percival S. M., Salaris M., 2011, 412, 2445
Peterson R. C., Dorman B., Rood R. T., 2001, ApJ, 559, 372
Price J., Phillipps S., Huxor A., Smith R. J., Lucey J. R., 2010, MNRAS, 412, 127
Rawle T. D., Smith R. J., Lucey J. R., Hudson M. J., Wegner G. A., 2008, MNRAS, 385, 2097
Ree C. H. et al., 2007, ApJS, 173, 607
Rich R. M. et al., 2005, ApJ, 619, L107
Salim S., Rich R. M., 2010, ApJ, 714, L290
Schiavon R. P., 2007, ApJS, 171, 146
Schiavon R. P., Rose J. A., Courteau S., MacArthur L. A., 2004, ApJ, 608, L33
Schlegel D. J., Finkbeiner D. P., Davis M., 1998, ApJ, 500, 525
Serra P., Trager S. C., 2007, MNRAS, 374, 769
Smith R. J., Lucey J. R., Hudson M. J., Allanson S. P., Bridges T. J., Hornschemeier A. E., Marzke R. O., Miller N. A., 2009, MNRAS, 392, 1265
Smith R. J. et al., 2010, MNRAS, 408, 1417
Smith R. J., Lucey J. R., Price J. A., Hudson M. J., Phillipps S., 2012, MNRAS, 419, 3167
Thomas D., Maraston C., Bender R., Mendes de Oliveira C., 2005, ApJ, 621, 673
Trager S. C., Worthey G., Faber S. M., Burstein D., Gonzalez J. J., 1998, ApJS, 116, 1
Trager S. C., Faber S. M., Worthey G., González J. J., 2000, AJ, 120, 165
Welch G. A., 1982, ApJ, 259, 77
Worthey G., 1998, PASP, 110, 888
Worthey G., Faber S. M., Gonzalez J. J., Burstein D., 1994, ApJS, 94, 687
Yi S. K., Demarque P., Kim Y.-C., 1997a, ApJ, 482, 677
Yi S. K., Demarque P., Oemler A., Jr, 1997b, ApJ, 486, 201
Yi S. K. et al., 2005, ApJ, 619, L111
Yi S. K., Lee J., Sheen Y.-K., Jeong H., Suh H., Oh K., 2011, ApJS, 195, 22

SUPPORTING INFORMATION

Additional Supporting Information may be found in the online version of this article:

Table 1. The galaxy properties used for the analysis in Section 3.
Table 2. The 10-arcsec-diameter-aperture magnitudes from which colours were derived for the analysis in Section 3.

Please note: Wiley-Blackwell are not responsible for the content or functionality of any supporting materials supplied by the authors. Any queries (other than missing material) should be directed to the corresponding author for the article.

This paper has been typeset from a TEX/LATEX file prepared by the author.